A comprehensive single-cell atlas of freshly dissociated human synovium in inflammatory arthritis with an optimized dissociation protocol for prospective fresh synovial biopsy collection

Sam G. Edalat[1,8], Reto Gerber[1,2,8], Miranda Houtman[1], Tadeja Kuret[1,3], Nadja Ižanc[1,3], Raphael Micheroli[1], Kristina Burki[1], Blaž Burja[1,3], Chantal Pauli[4], Žiga Rotar[3,5], Matija Tomšič[3,5], Saša Čučnik[3,6], Oliver Distler[1], Caroline Ospelt[1], Snežna Sodin-Semrl[3], Mark D. Robinson[2,*], Mojca Frank Bertoncelj[1,7,9,*]

[1]Center of Experimental Rheumatology, Department of Rheumatology, University Hospital Zurich and University of Zurich, 8952 Schlieren, Switzerland

[2]Department of Molecular Life Sciences and SIB Swiss Institute of Bioinformatics, University of Zurich, 8057 Zurich, Switzerland

[3]Department of Rheumatology, University Medical Centre Ljubljana, 1000 Ljubljana, Slovenia

[4]Department of Pathology, University Hospital Zurich, 8091 Zurich, Switzerland

[5]Faculty of Medicine, University of Ljubljana, 1000 Ljubljana, Slovenia

[6]Faculty of Medicine, University of Ljubljana, 1000 Ljubljana, Slovenia

[7]BioMed X Institute, Im Neuenheimer Feld 515, Heidelberg, Germany

[8]These authors contributed equally

[9]Lead contact

Correspondence:

*frankbertoncelj@bio.mx

*mark.robinson@mls.uzh.ch

Abstract

Single-cell RNA-sequencing is advancing our understanding of synovial pathobiology in inflammatory arthritis. Here, we optimized the protocol for dissociation of synovial biopsies and created a comprehensive reference single-cell atlas of fresh human synovium in inflammatory arthritis. We derived our protocol from the published dissociation method for cryopreserved synovium (Donlin L. et al. Arthritis Res. Ther. 2019) with modifications to enrich synovial cells and minimize cell loss. These modifications enabled consistently high cell yield and viability, thereby minimizing the rate of synovial tissue sample dropout. Our single-cell atlas of the human synovium comprised more than 100'000 unsorted single-cell profiles from 27 synovia of patients with inflammatory arthritis. Synovial cells formed ten lymphoid, 14 myeloid and 17 stromal cell clusters, including IFITM2+ synovial neutrophils. We identified lining SOD2^{high}SAA1+SAA2+ and transitional SERPINE1+COL5A3+ synovial fibroblasts, exhibiting gene signatures linked to cartilage breakdown (SDC4) and extracellular matrix remodelling (LOXL2, TGFBI, TGFB1), respectively. We uncovered synovial endothelial cell diversity and broadened the transcriptional characterization of tissue-resident FOLR2+ COLEC12+ and SLC40A1+ synovial macrophages, inferring their extracellular matrix sensing and iron recycling activities. Our research brings an efficient synovium dissociation protocol for prospectively collected fresh synovial biopsies and expands the knowledge about human synovium composition in inflammatory arthritis.

Keywords

synovium, arthritis, single-cell RNA sequencing, protocol, endothelial cells, fibroblasts, macrophages, neutrophils

Introduction

Chronic inflammatory arthritides, such as rheumatoid arthritis (RA) and the family of spondyloarthritides are clinically, radiologically, and molecularly diverse systemic autoimmune diseases that involve peripheral synovial joints and the axial skeleton[1,2]. They affect an important proportion of the world population and are associated with significant morbidity, lifelong disability, extraarticular manifestations and shorter life expectancwy[3–5]. Advances in therapy over the last decades have improved patient outcomes considerably and have pointed towards unique but also shared pathogenic pathways in different arthritis types[6,7]. Despite these advances, the management of inflammatory arthritides faces critical challenges, including the development of precision medicine, targeting the stromal cell compartment and discovering novel pro-resolution drugs[8–10].

The synovial tissue, a delicate inner layer of the joint capsule, is the primary disease site in inflammatory arthritides, while spondyloarthritis types affect also the entheses[11,12]. Given the central role of the synovium in inflammatory arthritides, understanding the identity and heterogeneity of its vital cellular components is quintessential in improving arthritis management and therapy[13,14]. Single-cell RNA-sequencing (scRNA-seq) paralleled with the advancement in minimally invasive synovial biopsy[15] has expanded our knowledge about synovial cell composition across arthritis types[16,17] and activity states[18] (e.g., remission vs flare). Furthermore, single-cell omics combined with functional experiments has been instrumental in establishing new concepts in inflammatory arthritis, including the break of synovial lining macrophage barrier[19] and divergent specialization of lining and sublining synovial fibroblasts into matrix-destructive and proinflammatory cell types[20,21].

Biobanking of viably frozen tissues simplifies retrospective sample selection and centralized tissue processing and scRNA-seq, decreasing the cost, minimizing batch effects, and facilitating the retrospective patient selection[16,22]. However, dissociating cryopreserved synovia may lead to inconsistent cell recovery and possible loss of sensitive, short-lived cell populations such as neutrophils, thereby introducing an inherent analysis bias. This bias

could be overcome by isolation and analysis of cells from fresh prospectively collected synovial tissue samples. To date, most synovial scRNA-seq studies were carried out on the RA synovium, mainly using viably cryopreserved synovial tissues or pre-sorted synovial cell types[16,18,23] and the protocol for dissociating cryopreserved synovia has been optimized by Donlin and colleagues[22]. The largest scRNA-seq dataset of the fresh RA synovium, published by Stephenson and colleagues, comprises more than 20'000 unsorted scRNAseq cell profiles from synovectomies of five RA patients[17].

The single cell omics study group at the Center of Experimental Rheumatology, University Hospital Zurich, Switzerland[24,25] investigates the pathobiology of human tissues affected by autoimmune diseases, with first research phase focusing on protocol optimization and establishment of tissue atlases. We have recently published an optimized dissociation protocol and scRNA-seq map of the fresh and cultured human skin[24]. In this paper, we present an optimized protocol for efficient dissociation of prospectively collected fresh synovial biopsies from patients with inflammatory arthritis. Furthermore, we created a reference single-cell atlas of fresh human synovium in inflammatory arthritis, serving as an annotation and research resource for the scientific community.

Methods

Patient recruitment

We enrolled 41 consecutive patients with different types of inflammatory arthritis, who were admitted to the Department of Rheumatology, University Hospital Zurich, Switzerland, for synovial biopsy and introduction/change of arthritis therapy. The ethic committee of the Canton Zurich, Switzerland, approved the collection and analysis of patient data and synovial tissues. All patients signed the informed consent for participation in the study before inclusion. The arthritis diagnosis was set at the time of admission and was based on classification criteria for different arthritis types[2,26,27] and clinical examination by

rheumatologist. UA diagnosis was set when arthritis did not meet criteria for any defined arthritis type. In total, we collected 44 synovial tissues from 20 patients with RA, 6 patients with spondyloarthritis, 6 patients with psoriatic arthritis, and 9 patients with UA. Two RA and one patient with spondyloarthritis donated biopsies from two different joints. These paired biopsies were processed as independent samples for downstream analyses. Synovial tissue samples originated from different joints, including knees (n=17), wrists (n=14), metacarpophalangeal joints (n=11) and sternoclavicular joints (n=2).

Ultrasound-guided synovial tissue biopsy

We obtained synovial tissue by the ultrasound-guided synovial biopsy using the Quick core 18G x 6cm or Quick Core 16G 9cm biopsy needles and GE Logiq S7 ultrasound instrument[28]. The biopsied joints were evaluated for synovitis immediately before the biopsy, and synovial tissue fragments were utilized for immunohistology, dissociation protocol optimization, scRNA-seq analysis or other downstream applications. Multiple synovial tissue fragments were collected from each donor.

Histological analysis

Synovial tissue was formalin-fixed and paraffin-embedded, sectioned (2µm) and stained with Hematoxylin-Eosin, Giemsa and Elastica van Gieson for Krenn's synovitis scoring[29] and definition of synovial pathotype[14]. The presence of the synovium in biopsied material was confirmed histologically in 42 donors, while being based on scRNA-seq analysis for samples 54B and 76. The pathotype analysis was performed for synovial tissues undergoing scRNA-sequencing analysis. Briefly, slides were deparaffinized and automatically stained with specific antibodies against synovial cell markers (PECAM-1, DAKO JC/70a, 1:10; CD20, Ventana Roche L26, prediluted; CD3, Leica LN10, 1:500; CD68, DAKO A/S PG-M1, 1:50; CD138, DAKO A/S, MI15, 1:30 and CD15, DAKO A/S Carb-3, 1:100). We used the HRP-based DAB staining for antigen visualization and performed pre-treatments according to the manufacturer's instructions (Ventana BenchMark).

Synovial cell isolation from fresh synovia

Synovial biopsies used for protocol optimization and scRNA-seq were submerged in sterile RPMI culture medium, transferred to the laboratory, and processed within 1-2 hours of collection. Forty-four fresh synovial biopsy samples were dissociated either with the protocol of Donlin et al.[22] (protocol 1, n=27), or our optimized protocol (protocol 2, n=17) derived from Donlin et al.[22] Briefly, synovial biopsies were minced and digested in a mixed enzymatic-mechanical dissociation including Liberase TL (Roche) and DNAse I (Roche); red blood cells were lysed (Red Blood Lysis buffer, Roche), and synovial cell pellets washed. For a detailed description of our protocol (protocol 2) and reagents see Supplementary Methods and Key resource Table. Cell counts and viability were determined using a manual (Neubauer, Trypan Blue) or automatic (Luna-FL, Dual Fluorescence Cell Counter, Logos BioSystems, Acridine Orange/PI, ThermoFisher) cell counting.

Study workflow

Among the 44 dissociated synovial tissue samples, five samples were utilized for other downstream applications, nine samples were discarded because of the compromised cell viability/yield and three samples were excluded because of the limited quality of scRNA-seq library/data. The final synovial scRNA-seq dataset included single cell profiles from 27 high-quality synovial cell suspensions obtained from patients with RA (n=16 biopsies), psoriatic arthritis (n=3), spondyloarthritis (n=5) and UA (n=3), prepared by either protocol 1 or protocol 2. These data were integrated to create a reference single cell atlas of the human synovium in inflammatory arthritis. For comparing the two dissociation protocols, we integrated scRNA-seq data from RA and PsA synovial tissue samples, which were evenly distributed between the two protocols. All spondyloarthritis synovia were dissociated with protocol 1 and all UA synovia with protocol 2.

Single-cell RNA-seq library preparation and sequencing

Synovial single-cell libraries were prepared using the 3’ v3.0 and 3’ v3.1 protocols and reagents from 10X Genomics according to the manufacturer’s instructions targeting the

encapsulation of up to 6000 cells. We created two independent paired libraries from samples 23, 26 and 28 as part of the quality control pipeline. The quality and quantity of cDNA and libraries were assessed with Agilent Bioanalyzer (Agilent Technologies). Diluted 10nM libraries were pooled in equimolar ratios, and the library pools were sequenced on the Illumina NovaSeq6000 sequencer (paired-end reads, R1=28, i7=8, R2=91, min. 40,000 - 50,000 reads/cell) at Functional Genomics Center Zurich, the University of Zurich and ETH Zurich, Switzerland. The sequencing of pooled scRNA-seq libraries was performed in multiple rounds; two library pools (**Table 1**) combined synovial and skin scRNA-seq samples, the latter being part of the skin protocol optimization project[24].

Bioinformatics analysis of scRNA-seq data

Transcript count tables were generated from fastq files using cellranger count {cellranger} (version 6.0.0) and the reference Genome GRCh38.p13 (transcripts from GENCODE Release 32[30] with genes coding for mitochondrial rRNA and tRNA, protein-coding RNA, rRNA and tRNA. Samples 23, 26 and 28 consisted of two independent libraries and were combined with cellranger aggr. Additionally, one of the libraries from sample 26 was resequenced and combined with the corresponding sample data to obtain a similar sequencing depth across libraries and samples. Pooling synovial and skin scRNA-seq[24] samples led to a limited barcode swapping[31] with subsequent detection of a minor keratinocyte cluster in the synovial cell dataset. The swapped molecules and empty droplets were removed at the beginning of the analysis using the R package DropletUtils[32,33]. The resulting filtered count matrix was then used for downstream analysis. No special enrichment for neutrophils was done[34]. The analysis was performed in R (version 4.0.3)[35] using Bioconductor (version 3.12)[36] packages. The preprocessing consisted of the following steps: (heterotypic) doublet detection and removal using scDblFinder[37], low-quality cell filtering using scuttle[38] and SampleQC[39]and normalization (log-transformed normalized expression values) using scuttle. Highly variable genes were selected using scran[40], dimensionality reduction was performed using PCA and intrinsicDimension[41] (selection of PCA components to keep). Integration of the data (batch correction) was done using batchelor[42] with evaluations of batch integration using

CellMixS[43]. Cell type assignment was done in sequential steps. We identified the main synovial cell types first and then assigned cell subtypes within the main cell types individually. The first step of the main cell annotation was graph-based clustering (shared nearest neighbor graph and louvain clustering) with bluster[44] followed by manual annotation (second step) with assistance from automatic cell type assignment using CellID[45], cluster-specific/enriched genes and known marker genes. Cell subtype annotation followed the same steps as the main cell type annotation, starting from highly variable gene selection and using only the respective cell subset. Marker genes were determined with pairwise Wilcoxon tests (using scran). We combined these marker genes with known cell markers and manually selected genes identified in the cluster comparison analysis based on the log-fold change expression (logFC>I1I) to create the heatmaps. Differential abundance analysis was conducted using edgeR[46]. Figures were generated with ggplot2[47] and ComplexHeatmap[48].

Data and code availability

The complete scRNA-seq dataset from 27 synovial tissue samples of patients with inflammatory arthritis is available in the ArrayExpress database (accession number E-MTAB-11791, https://www.ebi.ac.uk/arrayexpress/). The data from patients 28 and 50 have been previously deposited in the NCBI Gene Expression Omnibus as part of another publication[49] and are accessible through GEO SuperSeries accession number GSE181082. The code and instructions for the comparative analysis of scRNA-seq data generated by protocols 1 and 2 are available at https://retogerber.pages.uzh.ch/protocol_synovial. The code and instructions for the synovial single-cell atlas analysis are available at https://retogerber.pages.uzh.ch/synovialscrnaseq.

Results

Optimized dissociation protocol for fresh synovium minimizes the sample dropout rate

We derived our synovium dissociation protocol (protocol 2, **Suppl. Methods**) from the method of Donlin et al.[22] (protocol 1) and optimized this original protocol for dissociation of

fresh synovial biopsies. Specifically, we modified the original protocol to enhance the release of cells from small fresh synovial biopsies and minimize cell loss by refining the washing steps and volumes of reaction mixes (see **Suppl. Methods** for details). In total, we processed 27 and 17 synovial biopsies with protocols 1 and 2, respectively. Krenn synovitis scores, as a global measure of synovitis, did not significantly differ between protocol 1 and protocol 2 samples [protocol 1 median (range): 4 (2-9), protocol 2: 4 (2-6); p=0.7, two tailed Mann-Whitney test]. We isolated a higher number of cells from samples dissociated with protocol 2 (**Figure 1a**); both, the protocol 2 refinements and clinical heterogeneity of consecutively recruited patients could contribute to this difference. Notably, synovial cell suspensions, dissociated with protocol 2, demonstrated consistently high cell viability irrespective of isolated synovial cell yields (**Figure 1b**). Due to low cell yield and viability, we lost 33% (9/27, median 2500 viable cells, range 0-7100) of samples dissociated with protocol 1, but none of the samples dissociated with protocol 2. Overall, this data suggested that by slight modifications to the original protocol we could decrease cell loss during sample processing and thus minimize the dropout rate of prospectively collected fresh synovial biopsies for scRNA-seq analyses. For final confirmation of these observations, the same synovial biopsy would need to be processed in parallel with protocols 1 and 2.

The optimized protocol enables comprehensive mapping of the human synovium

To understand whether our modifications to the original dissociation protocol led to differences in the synovial scRNA-seq data, we next compared synovial scRNA-seq data generated by protocols 1 and 2. The comparative protocol analysis included 19 synovial tissue samples, thereby avoiding the diagnosis bias between the two protocols (see Methods for details). **Table 2** shows the basic histology characteristics of patient synovia and 10x Genomics chemistries for samples included in the comparative protocol analysis. We generated high-quality scRNA-seq data by both protocols as demonstrated by the QC analysis (**Suppl. Fig. 1**). Specifically, we filtered out low-quality cells with a low total number of counts, a low total number of detected genes and a high percentage of mitochondrial counts (**Suppl. Fig. 1a**). The median number of high-quality cells kept per sample was 4294,

with around 15000 detected genes per sample (**Suppl. Fig. 1b**). The distribution of the total number of counts per cell (**Suppl. Fig. 1c**) and the total number of detected genes per cell (**Suppl. Fig. 1d**) was similar between samples dissociated with protocols 1 and 2. These results demonstrated that both protocols enabled the generation of high-quality scRNA-seq data when using highly viable synovial single-cell suspensions.

We generated 78'597 high-quality scRNA-seq profiles from 19 synovial tissue samples that formed 11 principal synovial cell clusters comprising CD45+ lymphoid, CD45+ myeloid and CD45- stromal synovial cell subsets (**Fig. 2a**). The main synovial cell populations were heterogeneously distributed across patients' synovia (Fig. 2B); their abundances, however, did not differ between protocols 1 and 2 (**Fig. 2b, c**). While neutrophils were detected primarily in the protocol 2 data (**Fig. 2b, c**) and highly enriched in a subset of protocol 2 samples, their enrichment was not statistically significant.

The heatmap with top gene markers, specific for the 11 principal synovial cell populations, is shown in Figure 3. Specifically, we identified synovial CD3E+ T cells, CD79A+ CD79B+ B cells, proliferating CD79A+ XBP1+ TOP2A+ B cells/plasmablasts, CD14+ macrophages, LILRA4+ GZMB+ ITM2C+ plasmacytoid dendritic cells (DCs), CD1C+ FCER1A+ DCs, CLEC9A+ DCs, CPA3+ mast cells, IFITM2^{high} neutrophils, VWF+ endothelial cells (ECs), ACTA2+TAGLN+ pericytes/mural cells and COL1A1+ synovial fibroblasts (**Fig. 2a, Suppl. Fig. 2**). CD1C+ FCER1A+ and CLEC9A+ DCs co-clustered with synovial macrophages (**Fig. 2a, Suppl. Fig. 2**). Top neutrophil genes are shown in Suppl. Fig. 3. Synovial T cells, macrophages, ECs and synovial fibroblasts represented 3-58%, 6-60%, 3-22% and 7-80% of all synovial cells across the patient samples, constituting the most abundant synovial cells populations (**Figs. 2a, c**). Looking closer at these cell populations, we identified CD4+ T cells, CD8A+ NKG7+ T cells, CD3- NKG7+ natural killer cells (**Suppl. Fig. 4a**), tissue resident synovial macrophages (expressing *MERTK, TREM2 CD206/MRC1* genes, **Suppl. Fig. 4b**), infiltrating synovial macrophages (expressing *IL1B, CD48* genes, **Suppl. Fig. 4b**), LYVE1^{high}CCL21^{high} lymphatic ECs, vWF+ vascular ECs (**Suppl. Fig. 4c**), PRG4^{high}THY1^{low} lining synovial fibroblasts, and THY1+

PRG4^{low} sublining synovial fibroblasts expressing *GGT5, CXCL12 or DKK3* genes (**Suppl. Fig. 4d**).

Overall, we could comprehensively map all major and minor synovial cell populations with both protocols, inferring that our optimized protocol kept the comprehensiveness of the original protocol in detecting synovial cell diversity.

Generation of a single-cell atlas of fresh human synovium in inflammatory arthritis

In the next step, we integrated the scRNA-seq data from 27 synovial tissue samples of patients with inflammatory arthritis (see Methods for details), generated either with protocol 1 or 2, to build a single-cell atlas of freshly dissociated human synovium in inflammatory arthritis. **Table 3** shows the basic characteristics of patient synovia and 10x Genomics chemistries for synovial samples included in the human synovium atlas analysis. The QC analysis of the scRNA-seq data from the 27 samples is shown in **Suppl. Fig. 5**. After filtering the cells with a low total number of counts, low total number of detected genes and a high percentage of mitochondrial counts (**Suppl. Fig. 5a**), we kept 105'031 high-quality single-cell profiles (**Suppl. Fig. 5b**). The distribution of the total number of counts per cell and the total number of detected genes per cell across the 27 synovial tissue samples is shown on **Suppl. Figs. 5c, d**.

Our synovial single-cell atlas comprised eleven principal synovial cell clusters (**Suppl. Fig. 6a**), which replicated the lymphoid, myeloid, and stromal cell types identified in our comparative protocol analysis (**Fig. 2a**). The variable distribution of these principal cell types across patient synovia is presented in **Suppl. Fig. 6b, c**. The top 10 marker genes defining these principal lymphoid, myeloid and stromal synovial cell populations are shown in Suppl. Fig. 7. Lymphocytes T, macrophages, synovial fibroblasts and ECs represented the most abundant cell types (**Suppl. Figs. 6a-c**). We further subclustered these populations to understand their subset diversity and distribution in the synovium from patients with inflammatory arthritis.

Subcluster analysis uncovers the diversity of T cells in freshly dissociated human synovium

We profiled 24'097 cells comprising six CD3+ T cell clusters (1-3, 5-7) and one cluster of CD3- NK cells (cluster 4) (**Fig. 4a**). T cell and NK cell clusters varied considerably across patient's synovia (**Fig. 4b, c**). The selected key marker and cluster-enriched genes of T and NK cells are presented in **Fig. 4d** and **Suppl. Fig. 8a**. Specifically, the CD4+ TIGIT- T cell clusters (1, 5, 6) differed in the expression of CCR7, LEF1, and SELL transcripts (**Fig. 4a, d**). Meanwhile, CD4+ TIGIT+ CTLA4+ T cells (cluster 3) contained FOXP3+ and CXCL13+ PDCD1+ cell subsets (**Figs. 4a, d, Suppl. Fig. 8b**), suggestive of regulatory and peripheral/follicular CD4+ helper T cell phenotypes[16]. A small population of proliferating TOP2A+ CENPF+ CD4+ T cells co-clustered with cluster 3 lymphocytes (**Suppl. Fig. 8c**). The CD8+ CCL5+ T lymphocytes comprised NKG7^{low} GZMK+ cells (cluster 2) and NKG7+ T cells (cluster 7), separating further into cytotoxic NKG7+ GNLY^{high} GZMK^{low} and NKG7+ GNLY- GZMK^{high} cells (**Figs. 4a, c, Suppl. Fig. 8d**). CD8+ T cell subsets varied in the expression of GZMB and GZMH transcripts (**Suppl. Fig. 8d**). The NKG7^{high} GNLY+ NK cells (cluster 4) were GZMB^{high} and expressed abundantly Killer Cell Lectin like Receptor (KLRC1, KLRD1, KLRF1) transcripts (**Fig. 4d**).

Synovial fibroblast heterogeneity in freshly dissociated human synovium

Through our analysis, we identified eight COL1A1+ synovial fibroblast clusters (**Fig. 5a**) and further classified these cells based on their expression of the lining (PRG4) and sublining (THY1) fibroblast markers[23] (**Fig. 5a, Suppl. Fig. 9a**). Overall, the abundance of synovial fibroblast clusters varied significantly across patient synovia (**Fig. 5b, c**). The eight synovial fibroblast clusters represented lining PRG4^{high} THY1^{low} (cluster 5) and PRG4^{med} THY^{low} (cluster 4) synovial fibroblasts, transitional PRG4^{med} THY1$^{med/high}$ synovial fibroblasts (clusters 2, 6, 8) and PRG4^{low} THY1^{high} sublining synovial fibroblasts (clusters 1, 3, 7) (**Fig. 5a, Suppl. Fig. 9a**). The proliferating TOP2A+ CENPF+ synovial fibroblasts co-clustered with cluster 2 fibroblasts and contained both PRG4^{high} and THY+ cells (**Suppl. Fig. 9b**). The PRG4^{high} lining synovial fibroblasts were previously reported as enriched in osteoarthritis synovia and associated with matrix-degrading activities, while HLA-DRA+ sublining cells were found abundant in leukocyte-rich RA[16,20,21,23].

To further understand the synovial fibroblast diversity, we defined the key marker genes of the eight fibroblast clusters (**Suppl. Fig. 10**). The lining fibroblasts (clusters 4, 5) expressed CD55, ITGB8, MMP3 and CTRAC1 transcripts while being GAS6$^{neg/low}$ (**Suppl. Fig. 10**) as previously reported[16,18]. Cluster 5 cells were characteristically CLIC5+ HBEGF+ MMP1+ with specific expression of TWISTNB[50] (**Suppl. Fig. 10**). We identified a small new population of SOD2^{high} fibroblasts (cluster 4) uniquely expressing syndecan 4 (*SDC4*) and proinflammatory genes *SAA1, SAA2* and *CCL20* (**Fig. 5d, Suppl. Fig. 10**). Notably, SDC4 was reported to be prominently expressed in synovial lining cells in RA synovia[51]. Among the transitional fibroblasts, we uncovered a distinct SERPINE1+ COL5A3+ population (cluster 2), characterized by an extracellular matrix remodelling gene signature (*LOXL2, TGFBI, TGFB1*) (**Fig. 5e, Suppl. Fig. 10**). The PLTP^{high} HLA-DRA^{high} [16] cells (cluster 8) expressed transcripts linked to MHCII class antigen presentation (HLA-DRA, HLA-DRB1, HLA-DPB1, CD74, **Suppl. Figs. 10, 11a**). The sublining GGT5^{high} CXCL12 ^{high} FGF7+ fibroblasts (cluster 1) were enriched in the expression of IL6 and NOTCH3 (**Suppl. Figs. 10, 11b**), while containing a small population of C3^{high} CXCL14^{high} fibroblasts (**Fig. 5f, Suppl. Fig. 10**). Synovial fibroblasts in cluster 7 were also NOTCH3+ but GGT5^{low} (**Suppl. Fig. 10, 11b**); NOTCH3 and GGT5 expression were previously associated with periarterial localization of synovial fibroblast[23]. The cluster comparison analysis further inferred that transcriptome of cluster 7 cells largely overlapped with other sublining and transitional fibroblast clusters, including TNXB^{high} GFBP6+ FGFBP2+ (cluster 6) and CADM1^{high} ACAN+ (cluster 3) cells (**Fig. 5a, Suppl. Fig. 10**).

Synovial scRNA-seq analysis broadens gene signatures of synovial macrophage subsets

The synovial macrophage/DC cluster contained 36’419 CD45+ single cells distributed into CD14- CD64- CD11b- DC and CD14+ CD64+ CD11b+ macrophage clusters (**Fig. 6a, Suppl. Fig. 12**). The heatmap in **Suppl. Fig. 12** shows key marker and cluster-enriched genes expressed in these macrophage and DC clusters. Specifically, DC clusters included LYZ^{high} CD1C+ CLEC10A+ DCs (cluster 12), LAMP3+ IDO1+ DCs (cluster 13), CLEC9A+ CADM1+ CLNK+ DCs (cluster 2) and plasmacytoid LILRA4+ GZMB+ ITM2C+ DCs (cluster 6) (**Fig. 6a, Suppl. Fig. 12**).

Plasmacytoid DCs expressed TCF4, ZFAT and interferon pathway (IRF4, IRF7, IRF8, SOX4) genes. The nine CD14+ CD64+ CD11b+ synovial macrophage clusters, included three CCR2+ clusters (clusters 3, 7, 10) and six FOL2R+ clusters (clusters 1, 4, 5, 8, 9, 11) (**Fig. 6a, Suppl. Fig. 12**), inferring their tissue-infiltrating and tissue-resident origins[48], respectively.

Among the CCR2+ macrophages, we identified two CX3CR1+ subsets, including CD48^{high} S100A12+ PLAC8+ SELL+ CD52^{high} macrophages (cluster 3) and CD48^{low} CLEC10A+ GPR183+ ARL4C+ macrophages (cluster 7) (**Fig. 6a, Suppl. Fig. 12**). These CD163- MERTK- TREM2- CD206$^{low/neg}$ MARCO$^{low/neg}$ cells exhibited a rather overlapping transcriptional signature, however with a notable difference in transcript abundances. Specifically, genes linked to proinflammatory (*CD114, IL1B, S100A8, S100A9, FCAR, ITGAX*), angiogenesis-regulating (*VEGFA, EREG*), host defense (*FCN1, LYZ, PPIF, APOBEC3A, SLC11A, CD93*) but also anti-inflammatory (*IL1RN, FPR2*) functions were particularly highly expressed in cluster 3 synovial macrophages (**Suppl. Fig. 12**), previously reported as enriched in active RA[18]. The third CCR2+ macrophage subset represented SPP1+ MARCO+ TREM2+ macrophages (cluster 10). These cells were CD163^{med} MERTK^{low} CD206^{low} and demonstrated a limited transcriptional overlap with the CCR2+ CX3CR1+ macrophage subsets (**Fig. 6a, Suppl. Fig. 12**). SPP1+ macrophages were reported as enriched in RA synovitis[18] and bronchoalveolar lavage from patients with severe COVID[52]. Furthermore, SPP1-expressing hepatic lipid-associated macrophages were shown to derive from bone marrow, replacing Kupffer cells (KCs) in metabolic-associated fatty liver disease[53].

The FOL2R+ tissue-resident synovial macrophages were segregated into five main clusters of MERTK+ CD206+ cells, previously associated with remission maintenance in RA[18], and a minor cluster of MERTK- CD206- cells (cluster 11) with a variable expression of tissue-resident macrophage genes (**Fig. 6a, Suppl. Fig. 12**). FOL2R+ MERTK+ CD206+ macrophages expressed the genes encoding *CMKLR1*, the receptor for resolvin E[54], and *SLCO2B1* transporter, associated with macrophage identity[55]. These cells were further characterized by abundant expression of genes encoding scavenger receptors (*CD206, STAB1*[56], *CD163*),

complement components (*C1QA, C1QB, C1QC*), and molecules involved in efferocytosis (*MERTK, LGMN*[57]) and cholesterol/lipid trafficking (APOE) (**Suppl. Fig. 12**), pointing to tissue clearing and homeostatic functions. We further divided FOL2R+ MERTK+ CD206+ macrophages based on their expression of Collectin family member 12 (*COLEC12*) into COLEC12- (cluster 9) and COLEC12+ (clusters 1, 4, 5, 8) subsets (**Fig. 6a, Suppl. Fig. 12**). A scavenger receptor[58] COLEC12 is involved in the clearance of microbes, oxLDL[59] and myelin[60] and acts as a high-affinity ligand for the collagen domain binding receptor LAIR1[61]. Studies in mice showed that LAIR1 controls homeostatic and anti-tumor functions of monocytes and interstitial macrophages in the lungs via stromal sensing[61]. Synovial COLEC12- macrophages overlapped transcriptionally with FOLR2+ tissue-resident and CCR2+ tissue-infiltrating macrophages, inferring a transitional cell state. COLEC12+ tissue-resident macrophages expressed CCL18, CCL13 and NUPR1 (Suppl. Fig. 12), the regulators of lymphoid/myeloid cell trafficking[62,63] and ferroptosis[64], respectively. Among COLEC12+ macrophages, we annotated TIMD4- TREM2- LYVE1^{high} (cluster 1), TIMD4+ TREM2+ LYVE1^{med} (cluster 8) and TIMD4+ TREM2+ LYVE1^{low} (clusters 4, 5) subsets (**Fig. 6a**). While LYVE1 and TIMD4 have been associated with the perivascular location[65] and tissue residency[66], respectively, TREM2 has been linked to regenerative wound healing[67] and pro-tumorigenic macrophage functions[68]. Our scRNA-seq analysis demonstrated that TIMD4- TREM2- LYVE1^{high} macrophages were particularly enriched in CD209 and SELENOP, while expressing transcripts associated with coagulation (F13A1[69]), tissue-adaptation to stress (IGF1[70]), suppression of inflammatory genes (EGR1[71]) and iron recycling (SLC40A1[72,73]) (**Suppl. Fig. 12**). These genes were also expressed in TIMD4+ TREM2+ LYVE1^{med} macrophages, albeit at lower levels, while showing a limited expression in TIMD4+ TREM2+ LYVE1^{low} cells (**Suppl. Fig. 12**). Like other synovial cell types, the abundances of DC and macrophage subsets varied significantly across patient synovia (**Fig. 6b, c**).

Endothelial cell diversity in freshly dissociated human synovium in inflammatory arthritis

Our synovial scRNA-seq atlas contained 9560 PECAM+ synovial EC profiles forming eight distinct EC clusters (**Fig. 7a**). We identified pan-endothelial and subtype-specific EC

markers[57,58] and genes for the core EC functions (**Suppl. Fig. 13**). The eight EC clusters included LAPTM5+ PROX1+ LYVE1+ CCL21+ lymphatic ECs (cluster 1), proliferating TOP2A+ CENPF+ MKI67+ ECs (cluster 2), ACKR1+ venous ECs (clusters 5-8), SPP1+ KDR+ capillary ECs (cluster 4) and GJA4+ CLDN5+ arterial ECs (cluster 3) (**Fig. 7a, Suppl Fig. 13**). Venous ACKR1+ ECs represented the largest synovial EC population (Fig. 6A). Among them, we identified ACKR1^{med} VWF^{med} KDR^{low} SPARC^{high} CLU- ECs (cluster 7) with capillary and venous gene expression signatures (**Suppl. Fig. 13**), suggesting a transitional phenotype. The ACKR1^{high} VWF^{high} KDR- CLU+ ECs (clusters 5, 6, 8) expressed SELE (neutrophil adhesion), IL1R1 (IL1B response) and IRF1 (interferon signaling) transcripts. Clusters 5 and 8 were additionally IL6+ SOD2+ with high expression of *CCL2* and *TNFAIP3* genes in cluster 8 (**Suppl. Fig. 13**). SPP1+ KDR+ capillary ECs (cluster 4) were enriched for transcripts encoding basement membrane-associated collagens (COL4A1, COL4A2, COL15A1)[74] and plasmalemma vesicle associated protein (PLVAP) (Suppl. Fig. 13), a regulator of microvascular permeability and diaphragm formation within endothelial fenestrae[75]. Finally, arterial ECs (cluster 3) were characterized by the expression of tight[76] (*CLDN5*) and gap[77] (*GJA4*) junction genes as well as genes involved in endothelial barrier regulation (*RHOB*)[78], lymphatic vascular patterning (*SEMA3G*)[79], regulation of TGFB activity (*LTBP4*), lymphocyte trafficking (*ICAM2*) and chemotaxis (*CXCL12*) (**Suppl. Fig. 13**). The eight EC clusters were detectable in all patient samples, their abundancies however varied significantly across patient synovia (**Fig. 7b, c**).

A reference single-cell map of human synovium in inflammatory arthritis

As the final step in our analysis, we merged the cell annotations from the main cell types (**Suppl. Fig. 6a**) and their subsets (**Figs. 5-7**), identified in the integrated scRNA-seq dataset from 27 freshly dissociated synovia of patients with inflammatory arthritis. This analysis resulted in creating a comprehensive reference map of the human synovium, representing the synovial cell diversity in inflammatory arthritis (**Fig. 8**).

Discussion

Integrative single-cell omics analyses quickly expand our understanding of unique and shared cell types across human tissues in health and disease[80]. These analyses rely on isolating highly viable cells either from fresh or viably cryopreserved human tissues. Fresh tissue dissociation facilitates less biased tissue interrogation while relying on stable isolation of high-quality cells to prevent sample loss. Here, we utilized the elegant protocol of Donlin et al., optimized for dissociation of cryopreserved synovia[22], and refined it for dissociation of small fresh human synovial biopsies. We enhanced the release of synovial cells by gentle tissue massaging and minimized cell loss by optimizing the washing steps, and volumes of reaction mixes. These refinements were associated with consistent isolation of good yield of viable synovial cells, thereby minimizing the rate of fresh sample dropout. Given minute amounts of the biopsied material, we could not process paired tissue fragments from the same donor by both protocols for unequivocal protocol-to-protocol comparison. However, we confirmed by scRNA-seq analysis that our protocol enables thorough synovial cell mapping and can be reliably used for prospective scRNA-seq studies on the human synovium in inflammatory arthritis.

We detected a small population of IFITM2^{high} neutrophils in freshly dissociated synovia. The comparative protocol analysis pointed to the primary neutrophil detection in synovial biopsies digested with our optimized protocol. However, the heterogeneous clinical characteristics of consecutively recruited patients could significantly confound these observations. The integrative scRNA-seq analysis of 27 synovial tissue samples further inferred that the variable neutrophil detection is primarily donor-dependent. To further explore neutrophil abundances in human synovia, we aimed to integrate our and publicly available human synovial datasets. However, both the short lifespan and intrinsically small library sizes of human neutrophils[81] have challenged the analysis of neutrophil abundances in publicly available synovial scRNA-seq data, either created from cryopreserved

synovia/pre-sorted cells or available in the pre-processed form of the filtered count matrices[16–18,23].

Our study reproduced many previously described synovial fibroblast, myeloid and lymphoid transcriptional cell states[16–18,23], while expanding synovial cell heterogeneity to neutrophils. Furthermore, we identified a small population of lining SDC4+ synovial fibroblasts and transitional SERPINE1+ COL5A3+ synovial fibroblasts, while broadening the transcriptional characterization of transitional FOLR2+ COLEC12- and tissue-resident FOLR2+ COLEC12+ synovial macrophages. SDC4 has been closely linked to synovial fibroblast attachment/invasion into articular cartilage and cartilage breakdown[51,82,83], while COLEC12 and SLC40A1 were associated with macrophage extracellular matrix sensing[67] and regulation of iron homeostasis[72,73]. We observed a minor subset of C3^{high} CXCL14^{high} cells within the sublining GGT5^{high} CXCL12^{high} synovial fibroblast cluster. Notably, synovial fibroblasts were recently shown to drive the local inflammatory tissue priming in preclinical models of arthritis in a C3-dependent manner; the primed fibroblast appeared to upregulate both C3 and CXCL14 mRNA expression[84]. Future phenotypic and functional experiments should confirm whether these gene signatures also translate into subset specific synovial cell functions.

Differential enrichment of distinct cell types across patient synovia might drive different pathogenic pathways and contribute to the characteristic interpatient variability in therapeutic response to currently prescribed disease modifying antirheumatic drugs. Our in-depth analysis of synovial EC diversity in inflammatory arthritis demonstrated the shared contribution of GGT5+ synovial fibroblasts and ACKR1^{high} VWF ^{high} SELE+ venous EC subsets to the synovial production of IL6. The variable abundances of IL6-producing cell subsets across patient synovia may shape differential therapeutic response of arthritis patients to anti-IL6 therapies or JAK inhibitors. The future studies involving larger stratified patient cohorts will be essential to link synovial cell composition to variation in therapeutic response. Furthermore, such studies might contribute to the cell subtype-based and

molecular pathway-based patient stratification across and within different clinical types of inflammatory arthritis[85].

In conclusion, we refined the synovial dissociation protocol for prospectively collected fresh synovial biopsies and generated an extensive reference single-cell resource of freshly dissociated human synovium. Our results not only diversify the knowledge about synovial cell composition in inflammatory arthritis but could also facilitate future prospective single-cell omics studies on fresh human synovium.

Acknowledgements

We thank all the patients who donated synovial biopsies for the realization of this study and to Benvinda Campos Henriques for excellent technical support.

Funding

This study was funded by research grants of Vontobel Foundation, OPO-Foundation, Novartis Foundation for Biomedical Research and SNSF Research Grant No. 176061. Marie-Lou Ringgenberg Foundation, Stiftung für Rheumaforschung, Swiss Rheumatology Society, medAlumni, University Zurich.

Author contributions

S.G.E, R.G., M.D.R and M.F.B conceived the study, S.G.E, M.H., T.K, N.I., B.B., M.F.B, performed experiments**,** R.G., M.D.R conducted a bioinformatic analysis of scRNA-seq data, R.M., K.B. recruited the patients and collected clinical data, R.M. performed the ultrasound-guided synovial biopsy, Ž.R., M.T., S.Č., O.D., C.O., S.S.S, M.F.B were involved in study organization, C.P. performed immunohistology, S.G.E, R.G., M.D.R. and M.F.B analyzed and interpreted the data, S.G.E, R.G., M.H, M.F.B wrote the paper, all authors contributed to critical discussion and final drafting of the article, and agree with the paper content.

Declaration of interests

The authors declare no conflict of interests.

Figures

Figure 1. Number and viability of isolated synovial cells across synovial cell isolation protocols. Shown is the median. Protocol 1 – the original protocol of Donlin et al. Protocol 2 – the optimized protocol derived from Donlin et al. M, manual cell counting using the Neubauer chamber. A: automatic cell counting with the Luna-FL double fluorescence cell counter. Statistics: comparison of automatic measurements between the protocols with a two-tailed Mann-Whitney test, *p=0.03.

Figure 2. Comparative protocol analysis of scRNA-seq data. a) UMAP of the integrated scRNA-seq dataset with main synovial cell populations colored by main cell type. ScRNA-seq data generated from fresh human synovia, dissociated either with the original protocol of Donlin et al. (protocol 1) or the optimized protocol (protocol 2). **b)** Bar plots of relative abundances of main cell types per sample per protocol. **c)** The proportion of cell types per protocol 1 versus protocol 2; neutrophils were detected primarily in protocol 2 scRNA-seq data.

Figure 3. Top marker genes of the main synovial cell types identified in the comparative protocol scRNA-seq analysis. Shown is the heatmap with top 10 cell type marker genes. Expressions are aggregated by sample and cell type.

Figure 4. Subcluster analyses of synovial T cell populations within the integrated synovial single cell atlas of inflammatory arthritis comprising single cell scRNA-seq profiles from 27 patients with inflammatory arthritis (see Methods for details). a) UMAP with annotated T cell and NK cell subsets colored by cell subset, **b)** a bar plot of T cell subset abundances across synovial biopsies of patients with inflammatory arthritis colored by cell subset (right). **c)** the

proportions of the seven T cell subsets **d)** the heatmap of the top T cell and NK cell marker genes.

Figure 5. Subcluster analysis of synovial fibroblast populations within the integrated synovial single cell atlas of inflammatory arthritis comprising single cell scRNA-seq profiles from 27 patients with inflammatory arthritis (see Methods for details). a) UMAP with annotated synovial fibroblast subsets colored by cell subset. **b)** A bar plot of synovial fibroblast subset abundances across synovial biopsy samples of patients with inflammatory arthritis colored by cell subset (right). **c)** The proportions of the eight synovial fibroblast clusters across synovia from 27 patients with inflammatory arthritis. **d)** Violin plots showing the top enriched genes, expressed by the cluster 4 lining SOD2^{high} synovial fibroblasts, including *SDC4* and proinflammatory genes (*SAA1, SAA2, CCL20*). **e)** Violin plots showing the top enriched matrix-remodelling genes (*LOXL2, TGFBI, TGFB1*), expressed by the cluster 2 transitional SERPINE1+ COL5A3+ synovial fibroblasts. **f)** UMAPs demonstrating C3 and CXCL14 mRNA expression in synovial fibroblasts, identifying a small population of C3^{high} CXCL14^{high} cells within the sublining GGT5^{high} CXCL12^{high} synovial fibroblast subset (cluster 1).

Figure 6: Subcluster analysis of synovial macrophage and dendritic cell subsets in fresh human synovium in inflammatory arthritis. Macrophage annotations were performed on the integrated scRNA-seq dataset from 27 synovial tissue samples of patients with different types of inflammatory arthritis (see Methods for details). **a)** UMAP of four dendritic cell (DC) and nine infiltrating, transitional and tissue-resident synovial macrophage subsets colored by cell subset. **b)** Bar plots of relative abundances of four DC and nine synovial macrophage subsets across 27 patient samples colored by macrophage subset. **c)** The proportion of four DC and nine macrophage clusters across synovia from 27 patients with inflammatory arthritis.

Figure 7: Subcluster analysis of synovial endothelial cell subsets in fresh human synovium in inflammatory arthritis. Endothelial cell (EC) annotations were performed on the

integrated scRNA-seq dataset from 27 synovial tissue samples of patients with inflammatory arthritis (see Methods for details). **a)** UMAP of eight synovial EC subsets colored by EC subset. **b)** Barplots of relative abundances of eight EC subsets across 27 patient synovia colored by EC subset. **c)** The proportion of the eight EC clusters across 27 synovial tissue samples from patients with inflammatory arthritis.

Figure 8. Single-cell atlas of the freshly-dissociated human synovium in inflammatory arthritis. Comprehensive UMAP of annotated 10 lymphoid, 14 myeloid and 17 stromal cell populations and subpopulations showing extensive cellular heterogeneity of the human synovium in inflammatory arthritis. Cell annotations are based on the analysis of the main cell types and the subcluster analysis of synovial T/NK cell, fibroblast, macrophage and endothelial cell clusters. The integrated scRNA-seq data are derived from 27 synovial tissue samples from patients with different types of inflammatory arthritis (see Methods for details).

Tables

Table 1. Per sample percentage of reads discarded because of swapped barcodes together with the sequencing project id. Removal of swapped barcodes was performed for library pools o24300 and o24793, which contained scRNA-seq libraries from skin and synovium. Skin samples are part of another project and are not listed.

Table 2. Histology characteristics and 10x Genomics chemistries for 17 synovial tissue samples from patients with inflammatory arthritis included in the comparative analysis of scRNA-seq data between the original (protocol 1) and optimized (protocol 2) protocols. Numbers denote the biopsies processed. F: female, M: male, Pathotypes: DM: diffuse myeloid, LM: lymphoid myeloid, F: fibroid, pauci-immune, U: unclassified; *gender data not reported for 1 patient in protocol 2 cohort, **Krenn scoring based on 10 out of 13 synovial tissues in protocol 2 patient cohort. Statistics: Graph Pad Prism software, ***two-sided Fisher's exact test, ****two-sided Mann-Whitney t test, $p < 0.05$ accepted as statistically significant difference.

Table 3. Histology characteristics and 10x Genomics chemistries for 27 synovial tissue samples from patients with inflammatory arthritis included in the generation of the single-cell atlas of the fresh human synovium. Numbers denote the biopsies processed. F: female, M: male, DM: diffuse myeloid, LM: lymphoid myeloid, F: fibroid, pauci-immune, U: unclassified. *Donlin L. et al. Arthritis Res Ther 2019. **Gender data not reported for 1 patient in protocol 2 cohort, ***Krenn scoring based on 21 out of 27 synovial tissues.

Table 1

Sample	Proportion of reads discarded	Sequencing project
Syn_Bio_023	NA	o20549, o20550
Syn_Bio_026	NA	o20549, o20550, o23841
Syn_Bio_028	NA	o21475
Syn_Bio_049	NA	o21475
Syn_Bio_050	NA	o21475
Syn_Bio_053	NA	o23841
Syn_Bio_054A	NA	o23841
Syn_Bio_054B	NA	o23841
Syn_Bio_062	NA	o23841
Syn_Bio_064	NA	o23841
Syn_Bio_074	NA	o23841
Syn_Bio_076	NA	o23841
Syn_Bio_077a	NA	o23841
Syn_Bio_077b	NA	o23841
Syn_Bio_078	8.32%	o24300
Syn_Bio_079	3.00%	o24300
Syn_Bio_081	3.36%	o24300
Syn_Bio_083	3.09%	o24300
Syn_Bio_084	3.07%	o24300
Syn_Bio_087	5.54%	o24300
Syn_Bio_091	1.11%	o24793
Syn_Bio_092	0.99%	o24793
Syn_Bio_093	1.20%	o24793
Syn_Bio_096	1.14%	o24793
Syn_Bio_098a	1.20%	o24793
Syn_Bio_098b	1.40%	o24793
Syn_Bio_099	1.03%	o24793

Table 2

	Protocol 1 (n=6)	**Protocol 2 (n=13)**	**p value**
Gender*			0.25***
Female	6	8	
Male	0	4	
Age*			0.14****
Median (range)	71.5 (39 – 81)	56 (20–72)	
Krenn synovitis score**			0.32****
Median (range)	5 (2-9)	4 (2–6)	
Pathotype			NA
Diffuse myeloid	2	3	
Lympho-myeloid	2	6	
Fibroid	1	3	
Unclassified	1	1	
10x Genomics Chemistry			0.0005****
3’ v3.0	5	0	
3’ v3.1	1	13	

Table 3

	Number of biopsies
Protocol	
1: Original, Donlin L. et al.*	11
2: Refined, Edalat S. et al.	16
Sex**	
Female	19
Male	6
Age	
Median (range)	55.5 (20–81)
Krenn synovitis score***	
Median (range)	4 (2–9)
Pathotype	
Diffuse myeloid	10
Lympho-myeloid	9
Fibroid	5
Unclassified	3
10x Genomics Chemistry	
3’ v3.0	5
3’ v3.1	22

Supplementary Figures

Supplementary Figure 1. **Quality control of comparative protocol scRNA-seq analysis. a)** The number of genes vs. total counts per sample colored by filter (left) and percentage mitochondrial counts (right). **b)** The number of cells per sample (left) and per protocol (right), colored by the number of genes (top) and by the number of genes in at least 1% of cells (bottom). **c)** Distribution of counts per protocol (left) and per sample (right). **d)** Distribution of the number of genes per protocol (left) and per sample (right).

Supplementary Figure 2. UMAPs of integrated scRNA-seq data from comparative protocol analysis, color by key marker genes (*CD1C*, *FCER1A*, *CLEC9A*) of dendritic cells.

Supplementary Figure 3: The heatmap of major neutrophil genes, detected in the comparative protocol scRNA-seq analysis. Expressions are aggregated by sample and cell type.

Supplementary Figure 4. UMAPs of integrated scRNA-seq data from comparative protocol analysis. **a)** T cells/NK cells, color by key marker genes *CD3*, *CD4*, *CD8*, *NKG7*. **b)** Macrophages color by key marker genes *MERTK, TREM2, CD206/MRC1, IL1B, CD4*8. **c)** Endothelial cells, color by key marker genes *LYVE1, CCL21, VWF*. **d**) Synovial fibroblasts, color by key marker genes *PRG4, THY1, GGT5, CXCL12, DKK3*.

Supplementary Figure 5. Quality control of scRNA-seq analysis of the single cell atlas of fresh human synovium. **a)** A cell level summary of the total number of counts, the number of detected genes and the percentage of mitochondrial counts. The number of genes vs. total counts per sample colored by filter (left) and percentage mitochondrial counts (right). **b)** Sample summary statistics with the number of cells and number of detected genes after filtering of low-quality cells. The number of cells per sample colored by number of genes (top) and by number of genes in at least 1% of cells (bottom). **c)** Distribution of counts per sample. **d)** Distribution of number of genes per synovial tissue sample.

.

Supplementary Figure 6. Integrated scRNA-seq dataset from 27 synovial tissue samples from patients with inflammatory arthritis (see Methods for details). **a)** UMAP of annotated main synovial cell populations colored by main cell type. **b)** Bar plots of relative abundances of main cell types per sample colored by main cell type. **c)** The variability of the proportion of cell types across patient synovia.

Supplementary Figure 7. A heatmap of top marker genes of the main synovial cell types identified in the integrated scRNA-seq dataset across 27 synovial tissue samples from patients with inflammatory arthritis (see Methods for details). Expressions are aggregated by sample and cell type.

Supplementary Figure 8. a) A heatmap of the cluster-enriched genes of synovial T cell subsets in patients with inflammatory arthritides. The integrated scRNA-seq dataset consists of 27 synovial tissue samples from patients with different types of inflammatory arthritis (see Methods for details). Expressions are aggregated by sample and cell type. b) UMAPs demonstrating the expression of *FOXP3, PCDC1* and *CXCL13* genes in the TIGIT+ CTLA4+ T cells (cluster 3). **c)** UMAPs showing the small population of proliferating TOP2A+ CENPF+ CD4+ T cells within the cluster 3 T cells. D) UMAPs demonstrating the expression of granzyme (*GZMK, GZMB, GZMH*) and granulysin (*GNLY*) genes in CD8+ T cell subsets (clusters 2, 7).

Supplementary Figure 9. The integrated dataset from 27 synovial biopsies of patients with inflammatory arthritis (see Methods for details) with **a)** violin plots showing the expression (logcounts) of the lining marker PRG4 and the sublining marker THY1 across the eight synovial fibroblast clusters identified, and **b)** UMAPs showing the small population of proliferating TOP2A+ CENPF+ synovial fibroblasts, co-clustering with the cluster 2 transitional SERPINE1+ COL5A3+ synovial fibroblasts.

Supplementary Figure 10. A heatmap of the top cluster genes and known markers of synovial fibroblast subsets detected in the synovium of patients with inflammatory arthritides. The integrated scRNA-seq dataset consists of 27 synovial tissue samples from patients with different types of inflammatory arthritis (see Methods for details). Expressions are aggregated by sample and cell type.

Supplementary Figure 11. The integrated dataset from 27 synovial biopsies of patients with inflammatory arthritis (see Methods for details) with **a)** UMAPs showing the enriched expression of the genes involved in MHCII class mediated antigen presentation in HLA-DRA^{high} synovial fibroblasts (cluster 8), and **b)** UMAPs showing the enriched expression of *IL6* and *NOTCH3* genes in sublining GGT5+ synovial fibroblasts (clusters 1, 7).

Supplementary Figure 12. A heatmap of the top cluster genes and known marker genes of synovial macrophage subsets detected in the integrated scRNA-seq dataset from 27 synovial tissue samples of patients with different types of inflammatory arthritis (see Methods for details). Expressions are aggregated by sample and cell type.

Supplementary Figure 13. Heatmap of the top cluster genes and known markers of synovial endothelial cell subsets detected in the integrated scRNA-seq dataset from 27 synovial tissue samples of patients with different types of inflammatory arthritis (see Methods for details). Expressions are aggregated by sample and cell type.

Supplementary Methods

Step-by-step synovial tissue dissociation protocol

A) Digest synovial tissue

In this first step of the protocol, fresh synovial tissue is washed to remove the potential sources of non-synovial cell contamination, minced into small fragments, and dissociated into synovial cell suspension using the combined enzymatic-mechanical tissue dissociation protocol. *Critically, the volumes of digestion mixes are refined to minimize cell loss.*

Timing: 47min

1. Wash synovial biopsy fragments in D-PBS.
    a. Transfer the biopsied tissue fragments with sterile forceps onto a wet membrane of a 70 µm cell strainer sitting in a well of a 6-well plate, filled with 4 ml PBS.
    b. Transfer the strainer with tissue to neighboring wells with fresh 4ml D-PBS. Repeat this washing step 2x. Keep the tissue wet. Washing removes potential cell contaminants that do not originate from tissue.
2. Mince synovial tissue.
    a. Transfer tissue fragments into a 250µl pre-warmed RPMI (glutamine, HEPES, no Abs, no FBS) drop on a round bottom culture plate.
    b. Mince synovial tissue with a sterile scalpel into small tissue fragments (~1mm). Keep the tissue wet. Prepare digestion mix.
    c. Transfer 500µl of the pre-warmed RPMI medium (glutamine, HEPES, no Abs, no FBS) into a conical 15ml polystyrene tube. Add 40µl of 2.5mg/ml Liberase

TL, Roche to reach 100 µg/ml working Liberase TL concentration and 10µl of 10 mg/ml DNAse I, Roche to get 100 µg/ml working DNase I concentration.

d. Transfer the minced tissue fragments with a wide-bore pipette tip, forceps or scalpel into the digestion mix and top the volume with RPMI (glutamine, HEPES, no Abs, no FBS) to a total of 1ml. Collect all tissue fragments, which might stick to the tip, scalpel, or forceps surfaces. Avoid using the forceps with serrated surface to prevent excessive tissue sticking and tissue loss.

e. Add magnetic stirrer(s) in the tube and close the tube safely.

3. Digest synovial tissue at 37 °C in a mixed enzymatic-mechanical protocol.

   a. Transfer the tube with tissue fragments into a 37 °C water bath on a magnetic holder, placed within the prewarmed oven (37 °C). *The water bath facilitates keeping the suspension temperature at 37 °C during tissue digestion.*

   b. Digest tissue for 30 min at 37 °C with a continuous magnetic stirring. *A combination of a ball-shaped and a cylinder-shaped stirrers facilitates tissue mixing during digestion.*

   c. Fifteen minutes after starting the digestion, pass tissues gently through a 16G needle (10x) using a 1 ml syringe (mechanical dissociation).

      CRITICAL: The 16G needle may clog with tissue fragments; the built pressure may detach the needle, leading to tissue fragment/cell loss. The 1 ml syringe fits in the falcon tube, preventing the loss of cell suspension in case of needle detachment.

4. Stop the enzymatic digestion.

   a. Add 200µl of FBS and 800µl of RPMI (glutamine, HEPES, no Abs, no FBS) to the digestion mix to reach the final 10% FCS concentration.

B) Enrich dissociated synovial cells

In this step, tissue debris and cell aggregates are removed to obtain a single cell suspension of synovial cells. *Critically, the synovial cell suspension is enriched by releasing the remaining synovial cells from the digested tissue. Additional washes are introduced to minimize cell loss.*

Timing: 16 min

1. Pre-wet the 40µm strainer with 2ml of RPMI medium (glutamine, HEPES, no Abs, 10% FBS) in the six-well plate. Filter the cell suspension through the 40µm strainer submerged into the medium using 1ml wide-bore pipette tips.
2. *Wash the falcon tube with an additional 1ml of 10% RPMI to collect the remaining cells and filter through the pre-wet 40µm strainer into the well with filtered cell suspension.*
3. *Tissue debris and poorly disaggregated cell clumps will remain on the strainer. Using the syringe plunger head, gently press the synovial tissue fragments against the strainer to facilitate further cell release. Collect any remaining drops of cell suspension from the bottom side of the strainer with a fresh pipette tip and add to the filtered cell suspension.*

   CRITICAL: *This step releases additional cells from the tissue*.
4. *Transfer the 5ml of the filtered cell suspension into a new 15ml Falcon tube.*
5. *Wash the well with an additional 5ml of 10% RPMI to collect the remaining cells.*
6. Centrifuge the enriched filtered cell suspension at 300xg, RT, 10 min.

C) Lyse red blood cells

In this step, red blood cells are lysed, and synovial cells are washed.

Timing: 27 min

1. Lyse the red blood cells.
   a. During centrifugation, prepare 1x red cell lysis buffer (Roche) by mixing 0.5ml of 10x RBC Lysis Buffer in 4.5ml of nuclease-free H2O.
   b. Remove the supernatant and resuspend the pellet gently in 0.5ml RPMI containing 10% FCS.
   c. Add 5 ml of 1x RBC lysis buffer to the cells in 10% RPMI, vortex gently 5 sec, incubate 2 min RT.

   d. Centrifuge cell suspension at 300xg, RT, 10min. Remove the supernatant.

2. Wash the cells in D-PBS.
   a. Resuspend cells gently by flicking the pellet and then wash the cells with 10ml PBS. Centrifuge at 300xg RT, 10 min.
   b. Remove the supernatant.
   c. Centrifuge briefly at 300xg, RT to remove any residual solution.

D) Prepare single-cell suspension for scRNA-seq (10xGenomics)

In this step, the enriched cells are counted and checked for viability, potential remaining cell debris and aggregates are removed by additional filtering steps, and the suspension of single synovial cells is prepared for downstream applications (e.g., scRNA-seq).

Timing: 10 min.

1. Prepare fresh 0.2% BSA D-PBS (4µl of 50mg/ml BSA per 100µl D-PBS).
2. Gently flick the pellet and resuspend the cells with wide-bore tips in 100-150µl in 0.2% BSA D-PBS. Keep the cells on ice.
3. Using the, Count the cells, determine cell viability and check for debris or cell clumps (e.g, with Luna-FL dual fluorescence cell counter, Logos BioSystems). If remaining debris or cell clumps, filter the cell suspension through the 35µm strainer into 1.5ml Eppendorf tube.

   CRITICAL: This step helps preventing the clogging of the 10xGenomics chips.
4. Adjust the cell number to 700 single synovial cells/µl. Dilute or concentrate the cell suspension in 0.2% BSA D-PBS accordingly.

   CRITICAL: 700 cells/µl in our experience minimizes the probability of chip clogging.
5. Keep the cells on ice until starting with the 10x Genomics protocol

Key Resource Table

Reagents, commercial assays, consumables	SOURCE	IDENTIFIER
Dulbecco's Phosphate Buffered Saline	Thermo Fisher Scientific	Cat#14190144
RPMI 1640 medium, HEPES	Thermo Fisher Scientific	Cat#52400025
Liberase TL	Roche	Cat#05401020001
DNase I	Roche	Cat#11284932001
Fetal Bovine Serum	Corning	Cat#35-079-CV
Red Blood Cell lysis solution	Miltenyi Biotec	Cat#130-094-183
UltraPure™ DNase/RNase-free distilled water	Thermo Fisher Scientific	Cat#10977035
UltraPure™ BSA (50 mg/ml)	Thermo Fisher Scientific	Cat#AM2616
Acridin Orange PI	BioCat	F23002-LG
Chromium Controller & Next GEM accessory kit	10x Genomics	Cat#1000204
Chromium Next GEM Single Cell 3' GEM, library & gel bead kit v3.1, v3.0	10x Genomics	Cat#1000121
Chromium Next GEM Chip G single cell kit	10x Genomics	Cat#1000120
Single Index Kit T Set A	10x Genomics	Cat#1000213
6-well cell culture plate	TPP	Cat#92006
Cell strainer (70 µm)	Corning	Cat#352350
ART™ wide bore filtered pipette tips	Thermo Fisher Scientific	Cat#2069G
Tissue culture dish	TPP	Cat#93100
Scalpel	B. Braun	Cat#5518067
Tweezers		

15ml centrifuge tubes	TPP	Cat#91015
Magnetic stirring bar – ball shaped, micro		
Digital incubator 37°C		
Magnetic stirrer/squid		
Beaker (100ml)		
16-gauge blunt needle	Maybach	Cat#8001741
3 piece syringes (1ml)	BD Medical	Cat#303172
Cell strainer (40µm, 70µm)	Corning	Cat#352340
Centrifuge		
Luna-FL™ Dual Fluorescence counter	Logos Biosystems	

References

1. Feld, J., Chandran, V., Haroon, N., Inman, R. & Gladman, D. Axial disease in psoriatic arthritis and ankylosing spondylitis: a critical comparison. *Nature Reviews Rheumatology* **14**, 363–371 (2018).
2. Aletaha, D. *et al.* 2010 Rheumatoid arthritis classification criteria: an American College of Rheumatology/European League Against Rheumatism collaborative initiative. *Annals of the Rheumatic Diseases* **69**, 1580 (2010).
3. Karmacharya, P., Chakradhar, R. & Ogdie, A. The epidemiology of psoriatic arthritis: A literature review. *Best Practice & Research Clinical Rheumatology* **35**, 101692 (2021).
4. Gibofsky, A. Overview of epidemiology, pathophysiology, and diagnosis of rheumatoid arthritis. *Am J Manag Care* **18**, S295-302 (2012).
5. Stolwijk, C., van Onna, M., Boonen, A. & van Tubergen, A. Global prevalence of spondyloarthritis: a systematic review and meta-regression analysis. *Arthritis Care Res (Hoboken)* **68**, 1320–1331 (2016).
6. Veale, D. J. & Fearon, U. The pathogenesis of psoriatic arthritis. *The Lancet* **391**, 2273–2284 (2018).
7. Cantini, F. *et al.* Tailored first-line biologic therapy in patients with rheumatoid arthritis, spondyloarthritis, and psoriatic arthritis. *Seminars in Arthritis and Rheumatism* **45**, 519–532 (2016).
8. Pitzalis, C., Choy, E. H. S. & Buch, M. H. Transforming clinical trials in rheumatology: towards patient-centric precision medicine. *Nature Reviews Rheumatology* **16**, 590–599 (2020).
9. Schett, G. Resolution of inflammation in arthritis. *Seminars in Immunopathology* **41**, 675–679 (2019).
10. Siebert, S. *et al.* Targeting the rheumatoid arthritis synovial fibroblast via cyclin dependent kinase inhibition: An early phase trial. *Medicine* **99**, (2020).
11. Schett, G. *et al.* Enthesitis: from pathophysiology to treatment. *Nature Reviews Rheumatology* **13**, 731–741 (2017).
12. Orr, C. *et al.* Synovial tissue research: a state-of-the-art review. *Nature Reviews Rheumatology* **13**, 463–475 (2017).
13. Boutet, M.-A. *et al.* Interleukin-36 family dysregulation drives joint inflammation and therapy response in psoriatic arthritis. *Rheumatology* **59**, 828–838 (2020).
14. Humby, F. *et al.* Synovial cellular and molecular signatures stratify clinical response to csDMARD therapy and predict radiographic progression in early rheumatoid arthritis patients. *Ann Rheum Dis* **78**, 761–772 (2019).
15. Kelly, S. *et al.* Ultrasound-guided synovial biopsy: a safe, well-tolerated and reliable technique for obtaining high-quality synovial tissue from both large and small joints in early arthritis patients. *Annals of the Rheumatic Diseases* **74**, 611 (2015).

16. Zhang, F. *et al.* Defining inflammatory cell states in rheumatoid arthritis joint synovial tissues by integrating single-cell transcriptomics and mass cytometry. *Nature Immunology* **20**, 928–942 (2019).
17. Stephenson, W. *et al.* Single-cell RNA-seq of rheumatoid arthritis synovial tissue using low-cost microfluidic instrumentation. *Nature Communications* **9**, 791 (2018).
18. Alivernini, S. *et al.* Distinct synovial tissue macrophage subsets regulate inflammation and remission in rheumatoid arthritis. *Nature Medicine* **26**, 1295–1306 (2020).
19. Culemann, S. *et al.* Locally renewing resident synovial macrophages provide a protective barrier for the joint. *Nature* **572**, 670–675 (2019).
20. Croft, A. P. *et al.* Distinct fibroblast subsets drive inflammation and damage in arthritis. *Nature* **570**, 246–251 (2019).
21. Mizoguchi, F. *et al.* Functionally distinct disease-associated fibroblast subsets in rheumatoid arthritis. *Nature Communications* **9**, 789 (2018).
22. Donlin, L. T. *et al.* Methods for high-dimensional analysis of cells dissociated from cryopreserved synovial tissue. *Arthritis Res Ther* **20**, 139 (2018).
23. Wei, K. *et al.* Notch signalling drives synovial fibroblast identity and arthritis pathology. *Nature* **582**, 259–264 (2020).
24. Burja, B. *et al.* An Optimized Tissue Dissociation Protocol for Single-Cell RNA Sequencing Analysis of Fresh and Cultured Human Skin Biopsies. *Frontiers in Cell and Developmental Biology* **10**, (2022).
25. Micheroli, R. *et al.* Role of synovial fibroblast subsets across synovial pathotypes in rheumatoid arthritis: a deconvolution analysis. *RMD Open* **8**, e001949 (2022).
26. Rudwaleit, M. *et al.* The Assessment of SpondyloArthritis international Society classification criteria for peripheral spondyloarthritis and for spondyloarthritis in general. *Annals of the Rheumatic Diseases* **70**, 25 (2011).
27. Taylor, W. *et al.* Classification criteria for psoriatic arthritis: development of new criteria from a large international study. *Arthritis & Rheumatism: Official Journal of the American College of Rheumatology* **54**, 2665–2673 (2006).
28. Najm, A. *et al.* EULAR points to consider for minimal reporting requirements in synovial tissue research in rheumatology. *Ann Rheum Dis* (2022).
29. Krenn, V. *et al.* Grading of Chronic Synovitis — A Histopathological Grading System for Molecular and Diagnostic Pathology1 1The present work was supported by the SFB 421 (Project Z3: Protektive und pathologische Folgen der Antigenverarbeitung) and by Berlinflame (Project B2), BMBF. *Pathology - Research and Practice* **198**, 317–325 (2002).
30. Frankish, A. *et al.* GENCODE reference annotation for the human and mouse genomes. *Nucleic Acids Research* **47**, D766–D773.
31. Sinha, R. *et al. Index switching causes "spreading-of-signal" among multiplexed samples in Illumina HiSeq 4000 DNA sequencing*. https://www.biorxiv.org/content/10.1101/125724v1 (2021) doi:10.1101/125724.
32. Griffiths, J. A., Richard, A. C., Bach, K., Lun, A. T. L. & Marioni, J. C. Detection and removal of barcode swapping in single-cell RNA-seq data. *Nat. Commun.* **9**, 2667.

33. Lun, A. T. L. *et al.* EmptyDrops: distinguishing cells from empty droplets in droplet-based single-cell RNA sequencing data. *Genome Biol.* **20**, 63.
34. Capturing Neutrophils in 10x Single Cell Gene Expression DataCapturing Neutrophils in 10x Single Cell Gene Expression Data.
35. Team, R. C. *R: A Language and Environment for Statistical Computing*. (R Foundation for Statistical Computing).
36. Huber, W. *et al.* Orchestrating high-throughput genomic analysis with Bioconductor. *Nature Methods* **12**, 115–121 (2021).
37. Germain, P.-L., Lun, A., Macnair, W., Robinson, M. D. & F1000Research. *Doublet identification in single-cell sequencing data using scDblFinde r*. https://f1000research.com/articles/10-979 (2022) doi:10.12688/f1000research.73600.1.
38. McCarthy, D. J., Campbell, K. R., Lun, A. T. L. & Willis, Q. F. Scater: pre-processing, quality control, normalisation and visualisati on of single-cell RNA-seq data in R. *Bioinformatics* **33**, 1179–1186.
39. Macnair, W., Robinson, M. D. & bioRxiv. *SampleQC: robust multivariate, multi-celltype, multi-sample quality co ntrol for single cell data*. https://www.biorxiv.org/content/10.1101/2021.08.28.458012v1 (2022) doi:10.1101/2021.08.28.458012.
40. Lun, A. T. L., McCarthy, D. J. & Marioni, J. C. A step-by-step workflow for low-level analysis of single-cell RNA-seq data with Bioconductor. *F1000Res.* **5**, 2122.
41. Johnsson, K. Structures in High-Dimensional Data: Intrinsic Dimension and Cluster A nalysis. (Centre for Mathematical Sciences, Lund University).
42. Haghverdi, L., Lun, A. T. L., Morgan, M. D. & Marioni, J. C. Batch effects in single-cell RNA-sequencing data are corrected by matc hing mutual nearest neighbors. *Nat. Biotechnol.* **36**, 421–427.
43. Lütge, A. *et al.* CellMixS: quantifying and visualizing batch effects in single-cell RNA -seq data. *Life Science Alliance* **4**, (2022).
44. Lun, A. *bluster: Clustering Algorithms for Bioconductor*.
45. Cortal, A. & Rausell, A. *CellID: Unbiased Extraction of Single Cell Identity using Multiple Cor respondence Analysis*.
46. Robinson, M. D., McCarthy, D. J. & Smyth, G. K. edgeR: a Bioconductor package for differential expression analysis of digital gene expression data. *Bioinformatics* **26**, 139–140.
47. Wickham, H. *ggplot2: Elegant Graphics for Data Analysis*. (Springer-Verlag New York).
48. Gu, Z., Eils, R. & Schlesner, M. Complex heatmaps reveal patterns and correlations in multidimensional genomic data. *Bioinformatics*.
49. Morante-Palacios, O. *et al.* Coordinated glucocorticoid receptor and MAFB action induces tolerogenesis and epigenome remodeling in dendritic cells. *Nucleic Acids Res* **50**, 108–126 (2022).
50. Zhu, X. & Guo, W. Meta-Analyses of Multiple Gene Expression Profiles to Screen Hub Genes Related to Osteoarthritis. *Public Health Genomics* **24**, 267–279 (2021).

51. Godmann, L. *et al.* Antibody-mediated inhibition of syndecan-4 dimerisation reduces interleukin (IL)-1 receptor trafficking and signalling. *Annals of the Rheumatic Diseases* **79**, 481 (2020).
52. A, D. S. *et al.* Three tissue resident macrophage subsets coexist across organs with conserved origins and life cycles. *Science Immunology* **7**, eabf7777 (2022).
53. Remmerie, A. *et al.* Osteopontin Expression Identifies a Subset of Recruited Macrophages Distinct from Kupffer Cells in the Fatty Liver. *Immunity* **53**, 641-657.e14 (2020).
54. Trilleaud, C. *et al.* Agonist anti-ChemR23 mAb reduces tissue neutrophil accumulation and triggers chronic inflammation resolution. *Science Advances* **7**, eabd1453 (2022).
55. Park, I. *et al.* C-type lectin receptor CLEC4A2 promotes tissue adaptation of macrophages and protects against atherosclerosis. *Nature Communications* **13**, 215 (2022).
56. Pia, R. *et al.* Stabilin-1 expression defines a subset of macrophages that mediate tissue homeostasis and prevent fibrosis in chronic liver injury. *Proceedings of the National Academy of Sciences* **113**, 9298–9303 (2016).
57. Jia, D. *et al.* Cardiac Resident Macrophage-Derived Legumain Improves Cardiac Repair by Promoting Clearance and Degradation of Apoptotic Cardiomyocytes After Myocardial Infarction. *Circulation* **145**, 1542–1556 (2022).
58. Ma, Y. J. *et al.* Soluble Collectin-12 (CL-12) Is a Pattern Recognition Molecule Initiating Complement Activation via the Alternative Pathway. *The Journal of Immunology* **195**, 3365 (2015).
59. Ohtani, K. *et al.* The Membrane-type Collectin CL-P1 Is a Scavenger Receptor on Vascular Endothelial Cells *. *Journal of Biological Chemistry* **276**, 44222–44228 (2001).
60. Bogie, J. F. J. *et al.* Scavenger receptor collectin placenta 1 is a novel receptor involved in the uptake of myelin by phagocytes. *Scientific Reports* **7**, 44794 (2017).
61. Keerthivasan, S. *et al.* Homeostatic functions of monocytes and interstitial lung macrophages are regulated via collagen domain-binding receptor LAIR1. *Immunity* **54**, 1511-1526.e8 (2021).
62. Mendez-Enriquez, E. & Garcia-Zepeda, E. A. The multiple faces of CCL13 in immunity and inflammation. *Inflammopharmacology* **21**, 397–406 (2013).
63. Chenivesse, C. & Tsicopoulos, A. CCL18 – Beyond chemotaxis. *Cytokine* **109**, 52–56 (2018).
64. Liu, J. *et al.* NUPR1 is a critical repressor of ferroptosis. *Nature Communications* **12**, 647 (2021).
65. W, O. J. *et al.* Macrophages orchestrate the expansion of a proangiogenic perivascular niche during cancer progression. *Science Advances* **7**, eabg9518 (2022).
66. Dick, S. A. *et al.* Self-renewing resident cardiac macrophages limit adverse remodeling following myocardial infarction. *Nature Immunology* **20**, 29–39 (2019).
67. Dominic, H. *et al.* Xenogeneic skin transplantation promotes angiogenesis and tissue regeneration through activated Trem2+ macrophages. *Science Advances* **7**, eabi4528 (2022).

68. Molgora, M. *et al.* TREM2 Modulation Remodels the Tumor Myeloid Landscape Enhancing Anti-PD-1 Immunotherapy. *Cell* **182**, 886-900.e17 (2020).
69. Alshehri, F. S. M., Whyte, C. S. & Mutch, N. J. Factor XIII-A: An Indispensable "Factor" in Haemostasis and Wound Healing. *Int J Mol Sci* **22**, 3055 (2021).
70. Zaman, R. *et al.* Selective loss of resident macrophage-derived insulin-like growth factor-1 abolishes adaptive cardiac growth to stress. *Immunity* **54**, 2057-2071.e6 (2021).
71. Marco, T. *et al.* EGR1 is a gatekeeper of inflammatory enhancers in human macrophages. *Science Advances* **7**, eaaz8836 (2022).
72. Donovan, A. *et al.* The iron exporter ferroportin/Slc40a1 is essential for iron homeostasis. *Cell Metabolism* **1**, 191–200 (2005).
73. Theurl, I. *et al.* On-demand erythrocyte disposal and iron recycling requires transient macrophages in the liver. *Nature Medicine* **22**, 945–951 (2016).
74. Rowe, R. G. & Weiss, S. J. Breaching the basement membrane: who, when and how? *Trends in Cell Biology* **18**, 560–574 (2008).
75. Guo, L., Zhang, H., Hou, Y., Wei, T. & Liu, J. Plasmalemma vesicle-associated protein: A crucial component of vascular homeostasis. *Exp Ther Med* **12**, 1639–1644 (2016).
76. Otani, T. & Furuse, M. Tight Junction Structure and Function Revisited. *Trends in Cell Biology* **30**, 805–817 (2020).
77. Dhein, S. Gap junction channels in the cardiovascular system: pharmacological and physiological modulation. *Trends in Pharmacological Sciences* **19**, 229–241 (1998).
78. Marcos-Ramiro, B. *et al.* RhoB controls endothelial barrier recovery by inhibiting Rac1 trafficking to the cell border. *Journal of Cell Biology* **213**, 385–402 (2016).
79. Liu, X., Uemura, A., Fukushima, Y., Yoshida, Y. & Hirashima, M. Semaphorin 3G Provides a Repulsive Guidance Cue to Lymphatic Endothelial Cells via Neuropilin-2/PlexinD1. *Cell Reports* **17**, 2299–2311 (2016).
80. null, null *et al.* The Tabula Sapiens: A multiple-organ, single-cell transcriptomic atlas of humans. *Science (1979)* **376**, eabl4896 (2022).
81. Hay, S. B., Ferchen, K., Chetal, K., Grimes, H. L. & Salomonis, N. The Human Cell Atlas bone marrow single-cell interactive web portal. *Experimental Hematology* **68**, 51–61 (2018).
82. M, D. K. *et al.* Targeting phosphatase-dependent proteoglycan switch for rheumatoid arthritis therapy. *Science Translational Medicine* **7**, 288ra76-288ra76 (2015).
83. Korb-Pap, A. *et al.* Early structural changes in cartilage and bone are required for the attachment and invasion of inflamed synovial tissue during destructive inflammatory arthritis. *Annals of the Rheumatic Diseases* **71**, 1004 (2012).
84. Friščić, J. *et al.* The complement system drives local inflammatory tissue priming by metabolic reprogramming of synovial fibroblasts. *Immunity* **54**, 1002-1021.e10 (2021).
85. Zhang, F. *et al.* Cellular deconstruction of inflamed synovium defines diverse inflammatory phenotypes in rheumatoid arthritis. *bioRxiv* 2022.02.25.481990 (2022) doi:10.1101/2022.02.25.481990.

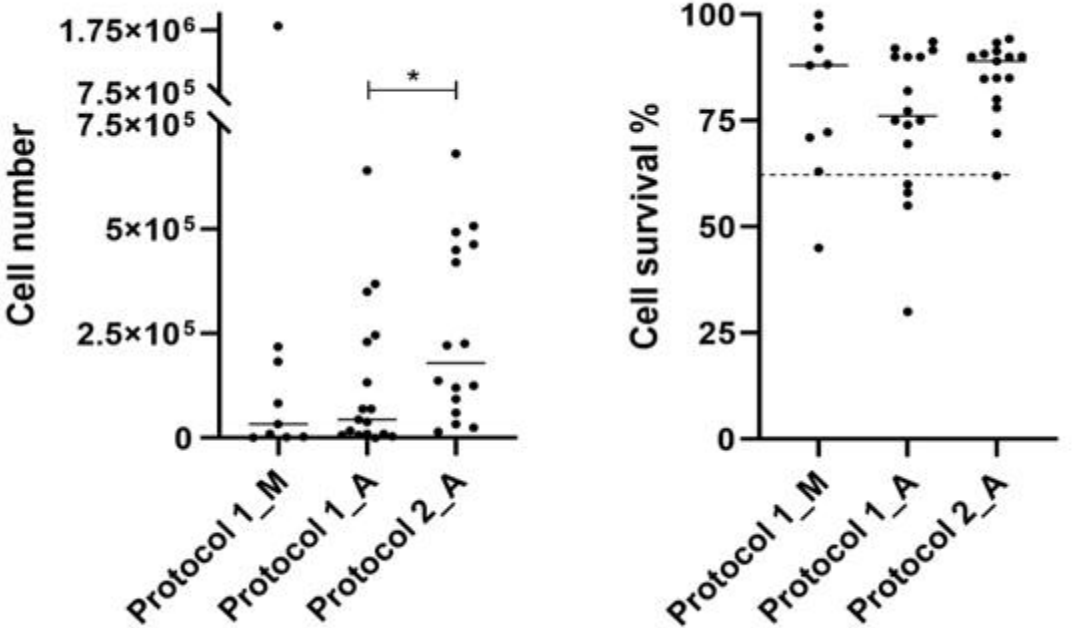
Cell number
1.75×10⁶
7.5×10⁵
7.5×10⁵
5×10⁵
2.5×10⁵
0
*
Protocol 1_M
Protocol 1_A
Protocol 2_A
Cell survival %
100
75
50
25
0
Protocol 1_M
Protocol 1_A
Protocol 2_A

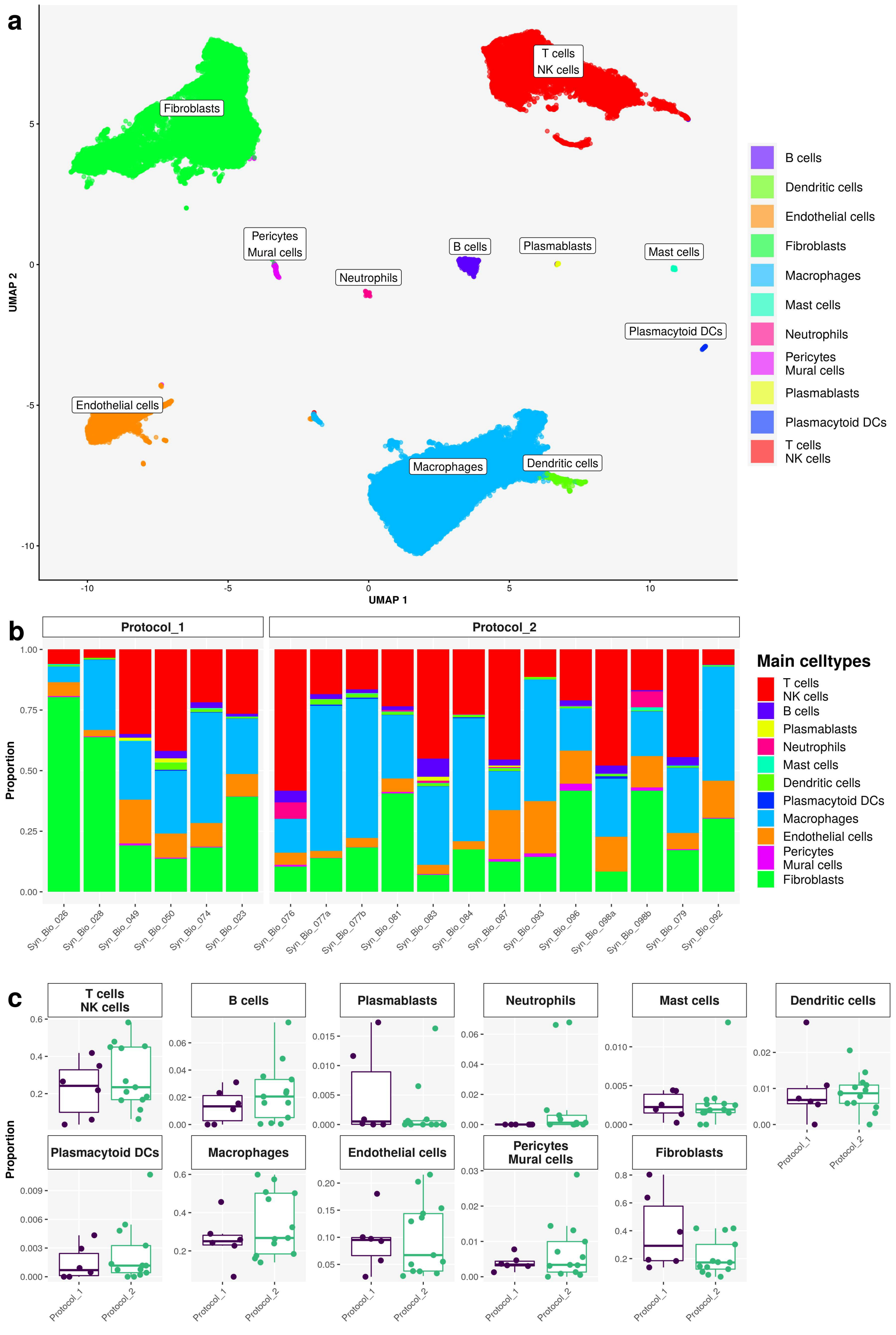
a
Fibroblasts
T cells
NK cells
Pericytes
Mural cells
B cells
Plasmablasts
Mast cells
Neutrophils
Plasmacytoid DCs
Endothelial cells
Macrophages
Dendritic cells
UMAP 2
UMAP 1
B cells
Dendritic cells
Endothelial cells
Fibroblasts
Macrophages
Mast cells
Neutrophils
Pericytes
Mural cells
Plasmablasts
Plasmacytoid DCs
T cells
NK cells
b
Protocol_1
Protocol_2
Proportion
Main celltypes
T cells
NK cells
B cells
Plasmablasts
Neutrophils
Mast cells
Dendritic cells
Plasmacytoid DCs
Macrophages
Endothelial cells
Pericytes
Mural cells
Fibroblasts
Syn_Bio_026
Syn_Bio_028
Syn_Bio_049
Syn_Bio_050
Syn_Bio_074
Syn_Bio_023
Syn_Bio_076
Syn_Bio_077a
Syn_Bio_077b
Syn_Bio_081
Syn_Bio_083
Syn_Bio_084
Syn_Bio_087
Syn_Bio_093
Syn_Bio_096
Syn_Bio_098a
Syn_Bio_098b
Syn_Bio_079
Syn_Bio_092
c
T cells
NK cells
B cells
Plasmablasts
Neutrophils
Mast cells
Dendritic cells
Plasmacytoid DCs
Macrophages
Endothelial cells
Pericytes
Mural cells
Fibroblasts
Proportion
Protocol_1
Protocol_2

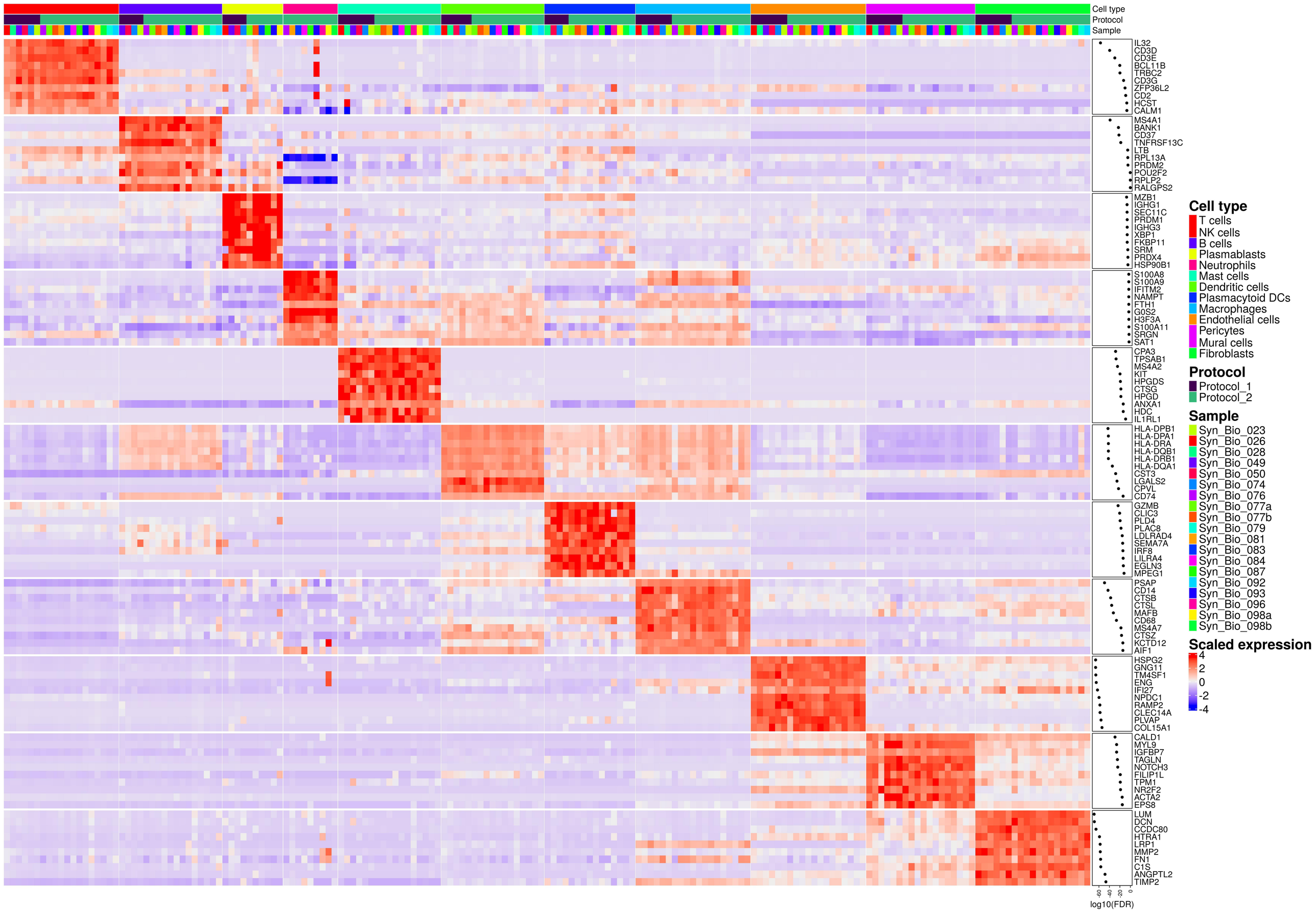
Cell type
Protocol
Sample
IL32
CD3D
CD3E
BCL11B
TRBC2
CD3G
ZFP36L2
CD2
HCST
CALM1
MS4A1
BANK1
CD37
TNFRSF13C
LTB
RPL13A
PRDM2
POU2F2
RPLP2
RALGPS2
MZB1
IGHG1
SEC11C
PRDM1
IGHG3
XBP1
FKBP11
SRM
PRDX4
HSP90B1
S100A8
S100A9
IFITM2
NAMPT
FTH1
G0S2
H3F3A
S100A11
SRGN
SAT1
CPA3
TPSAB1
MS4A2
KIT
HPGDS
CTSG
HPGD
ANXA1
HDC
IL1RL1
HLA-DPB1
HLA-DPA1
HLA-DRA
HLA-DQB1
HLA-DRB1
HLA-DQA1
CST3
LGALS2
CPVL
CD74
GZMB
CLIC3
PLD4
PLAC8
LDLRAD4
SEMA7A
IRF8
LILRA4
EGLN3
MPEG1
PSAP
CD14
CTSB
CTSL
MAFB
CD68
MS4A7
CTSZ
KCTD12
AIF1
HSPG2
GNG11
TM4SF1
ENG
IFI27
NPDC1
RAMP2
CLEC14A
PLVAP
COL15A1
CALD1
MYL9
IGFBP7
TAGLN
NOTCH3
FILIP1L
TPM1
NR2F2
ACTA2
EPS8
LUM
DCN
CCDC80
HTRA1
LRP1
MMP2
FN1
C1S
ANGPTL2
TIMP2
-60
-40
-20
0
log10(FDR)
Cell type
T cells
NK cells
B cells
Plasmablasts
Neutrophils
Mast cells
Dendritic cells
Plasmacytoid DCs
Macrophages
Endothelial cells
Pericytes
Mural cells
Fibroblasts
Protocol
Protocol_1
Protocol_2
Sample
Syn_Bio_023
Syn_Bio_026
Syn_Bio_028
Syn_Bio_049
Syn_Bio_050
Syn_Bio_074
Syn_Bio_076
Syn_Bio_077a
Syn_Bio_077b
Syn_Bio_079
Syn_Bio_081
Syn_Bio_083
Syn_Bio_084
Syn_Bio_087
Syn_Bio_092
Syn_Bio_093
Syn_Bio_096
Syn_Bio_098a
Syn_Bio_098b
Scaled expression
4
2
0
-2
-4

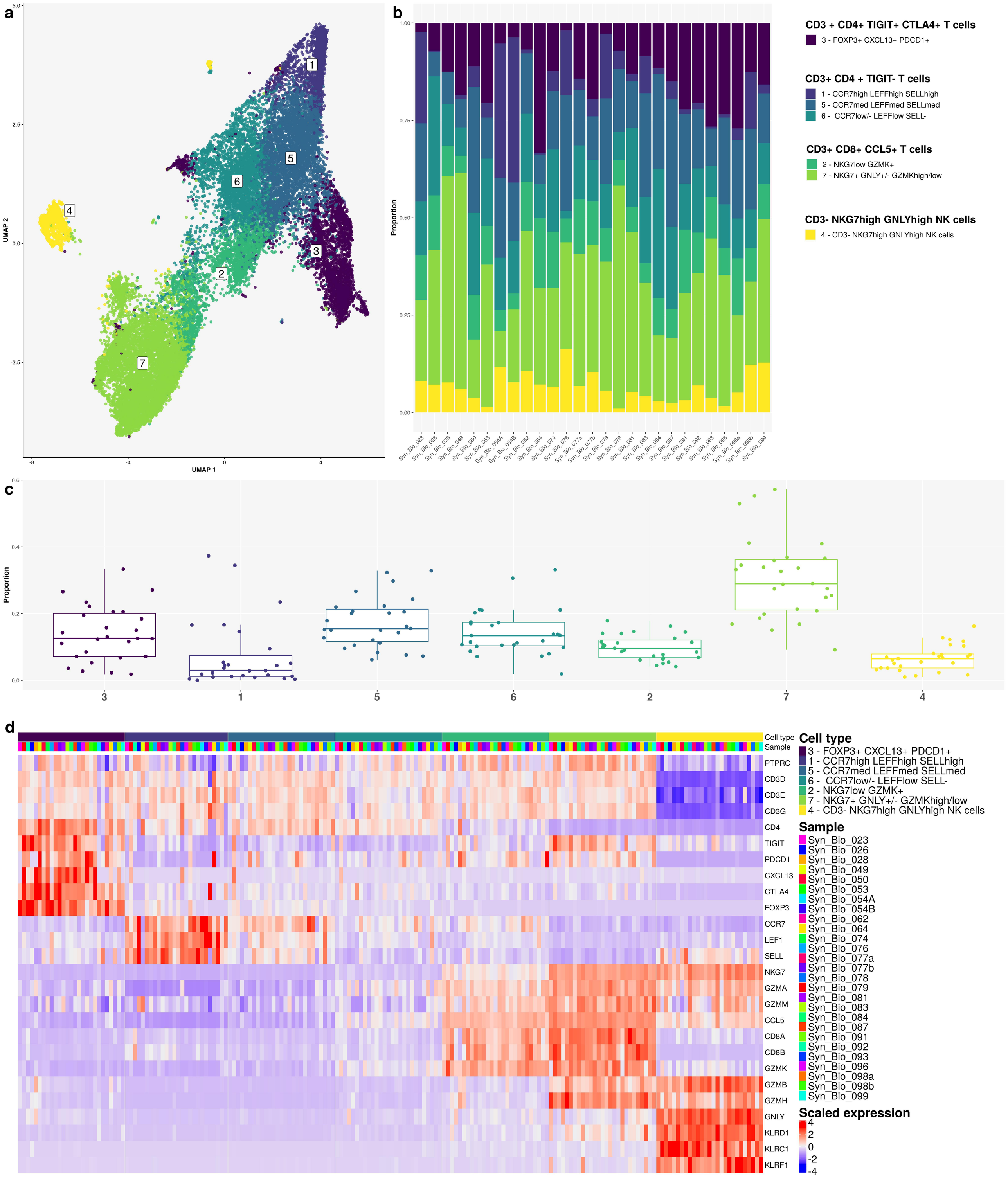
a
UMAP 2
UMAP 1
1
2
3
4
5
6
7
b
Proportion
CD3 + CD4+ TIGIT+ CTLA4+ T cells
3 - FOXP3+ CXCL13+ PDCD1+
CD3+ CD4 + TIGIT- T cells
1 - CCR7high LEFFhigh SELLhigh
5 - CCR7med LEFFmed SELLmed
6 - CCR7low/- LEFFlow SELL-
CD3+ CD8+ CCL5+ T cells
2 - NKG7low GZMK+
7 - NKG7+ GNLY+/- GZMKhigh/low
CD3- NKG7high GNLYhigh NK cells
4 - CD3- NKG7high GNLYhigh NK cells
c
Proportion
3
1
5
6
2
7
4
d
Cell type
Sample
PTPRC
CD3D
CD3E
CD3G
CD4
TIGIT
PDCD1
CXCL13
CTLA4
FOXP3
CCR7
LEF1
SELL
NKG7
GZMA
GZMM
CCL5
CD8A
CD8B
GZMK
GZMB
GZMH
GNLY
KLRD1
KLRC1
KLRF1
Cell type
3 - FOXP3+ CXCL13+ PDCD1+
1 - CCR7high LEFFhigh SELLhigh
5 - CCR7med LEFFmed SELLmed
6 - CCR7low/- LEFFlow SELL-
2 - NKG7low GZMK+
7 - NKG7+ GNLY+/- GZMKhigh/low
4 - CD3- NKG7high GNLYhigh NK cells
Sample
Syn_Bio_023
Syn_Bio_026
Syn_Bio_028
Syn_Bio_049
Syn_Bio_050
Syn_Bio_053
Syn_Bio_054A
Syn_Bio_054B
Syn_Bio_062
Syn_Bio_064
Syn_Bio_074
Syn_Bio_076
Syn_Bio_077a
Syn_Bio_077b
Syn_Bio_078
Syn_Bio_079
Syn_Bio_081
Syn_Bio_083
Syn_Bio_084
Syn_Bio_087
Syn_Bio_091
Syn_Bio_092
Syn_Bio_093
Syn_Bio_096
Syn_Bio_098a
Syn_Bio_098b
Syn_Bio_099
Scaled expression

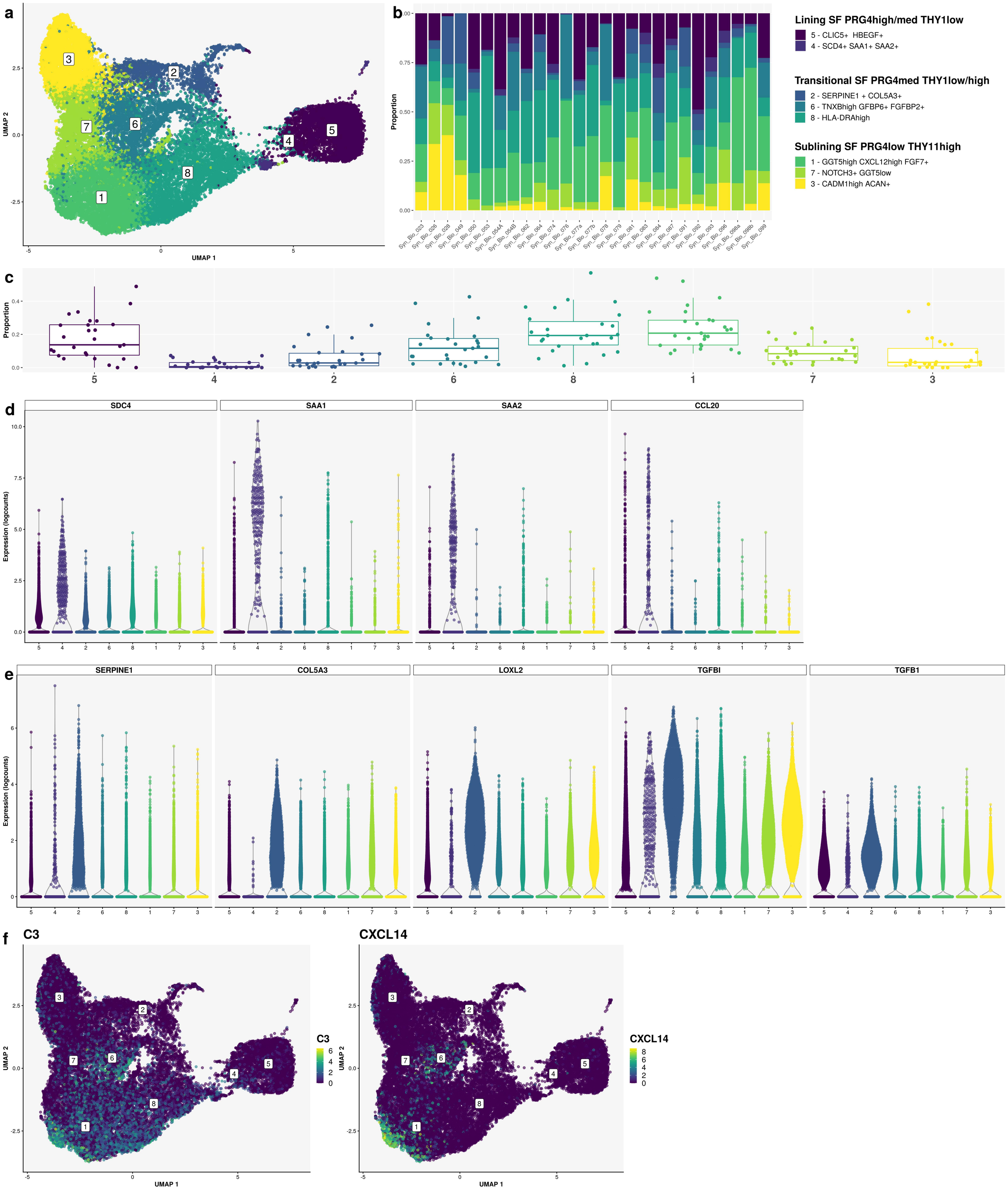
a
UMAP 1
UMAP 2
b
Proportion
Lining SF PRG4high/med THY1low
5 - CLIC5+ HBEGF+
4 - SCD4+ SAA1+ SAA2+
Transitional SF PRG4med THY1low/high
2 - SERPINE1 + COL5A3+
6 - TNXBhigh GFBP6+ FGFBP2+
8 - HLA-DRAhigh
Sublining SF PRG4low THY11high
1 - GGT5high CXCL12high FGF7+
7 - NOTCH3+ GGT5low
3 - CADM1high ACAN+
c
Proportion
d
SDC4
SAA1
SAA2
CCL20
Expression (logcounts)
e
SERPINE1
COL5A3
LOXL2
TGFBI
TGFB1
Expression (logcounts)
f
C3
CXCL14
UMAP 1
UMAP 2

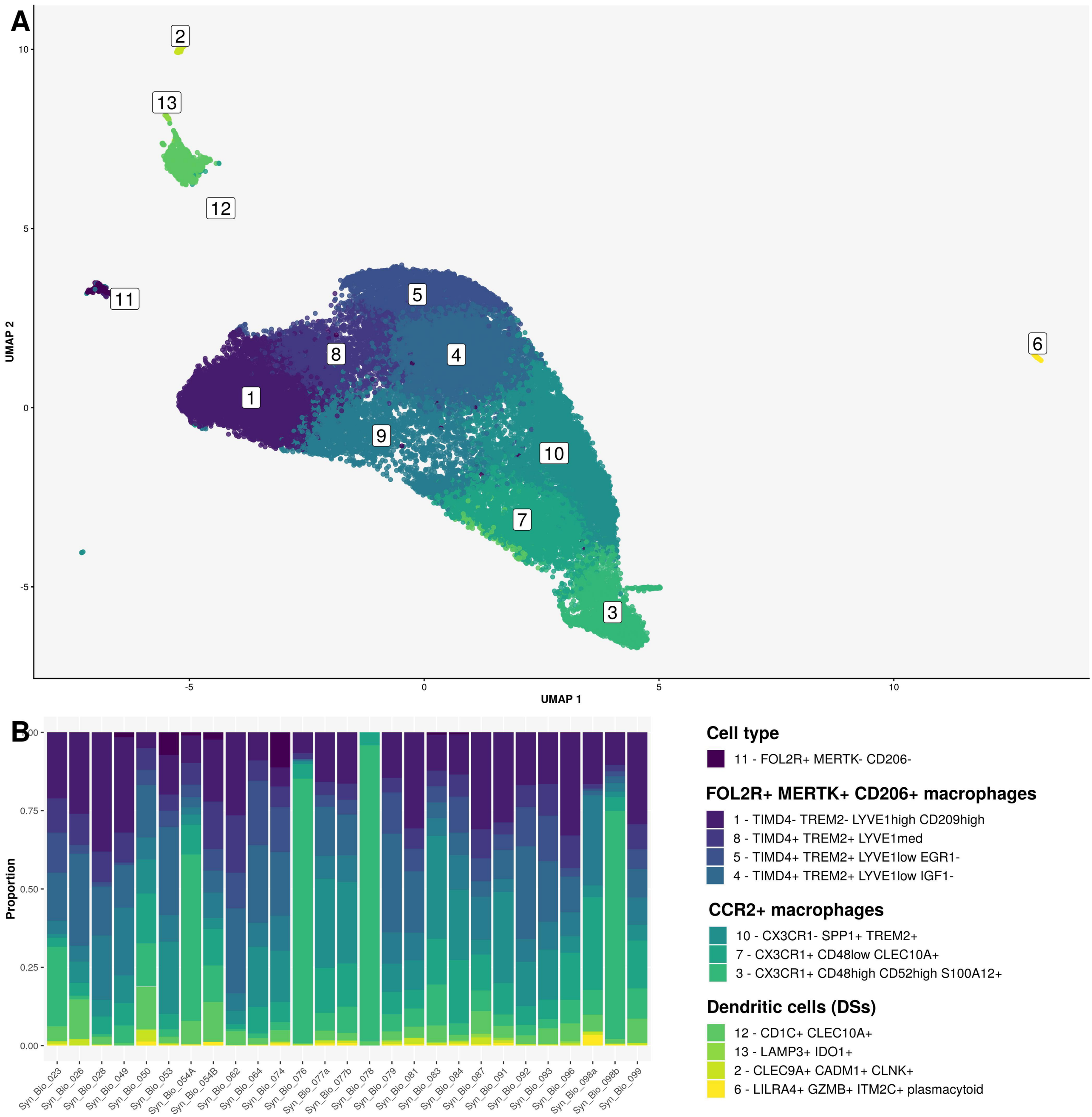
A
UMAP 2
UMAP 1
10
5
0
-5
-5
0
5
10
1
2
3
4
5
6
7
8
9
10
11
12
13
B
Proportion
1.00
0.75
0.50
0.25
0.00
Syn_Bio_023
Syn_Bio_026
Syn_Bio_028
Syn_Bio_049
Syn_Bio_050
Syn_Bio_053
Syn_Bio_054A
Syn_Bio_054B
Syn_Bio_062
Syn_Bio_064
Syn_Bio_074
Syn_Bio_076
Syn_Bio_077a
Syn_Bio_077b
Syn_Bio_078
Syn_Bio_079
Syn_Bio_081
Syn_Bio_083
Syn_Bio_084
Syn_Bio_087
Syn_Bio_091
Syn_Bio_092
Syn_Bio_093
Syn_Bio_096
Syn_Bio_098a
Syn_Bio_098b
Syn_Bio_099
Cell type
11 - FOL2R+ MERTK- CD206-
FOL2R+ MERTK+ CD206+ macrophages
1 - TIMD4- TREM2- LYVE1high CD209high
8 - TIMD4+ TREM2+ LYVE1med
5 - TIMD4+ TREM2+ LYVE1low EGR1-
4 - TIMD4+ TREM2+ LYVE1low IGF1-
CCR2+ macrophages
10 - CX3CR1- SPP1+ TREM2+
7 - CX3CR1+ CD48low CLEC10A+
3 - CX3CR1+ CD48high CD52high S100A12+
Dendritic cells (DSs)
12 - CD1C+ CLEC10A+
13 - LAMP3+ IDO1+
2 - CLEC9A+ CADM1+ CLNK+
6 - LILRA4+ GZMB+ ITM2C+ plasmacytoid
C
Proportion
0.75
0.50
0.25
0.00
11
1
8
5
4
9
10
7
3
12
13
2
6

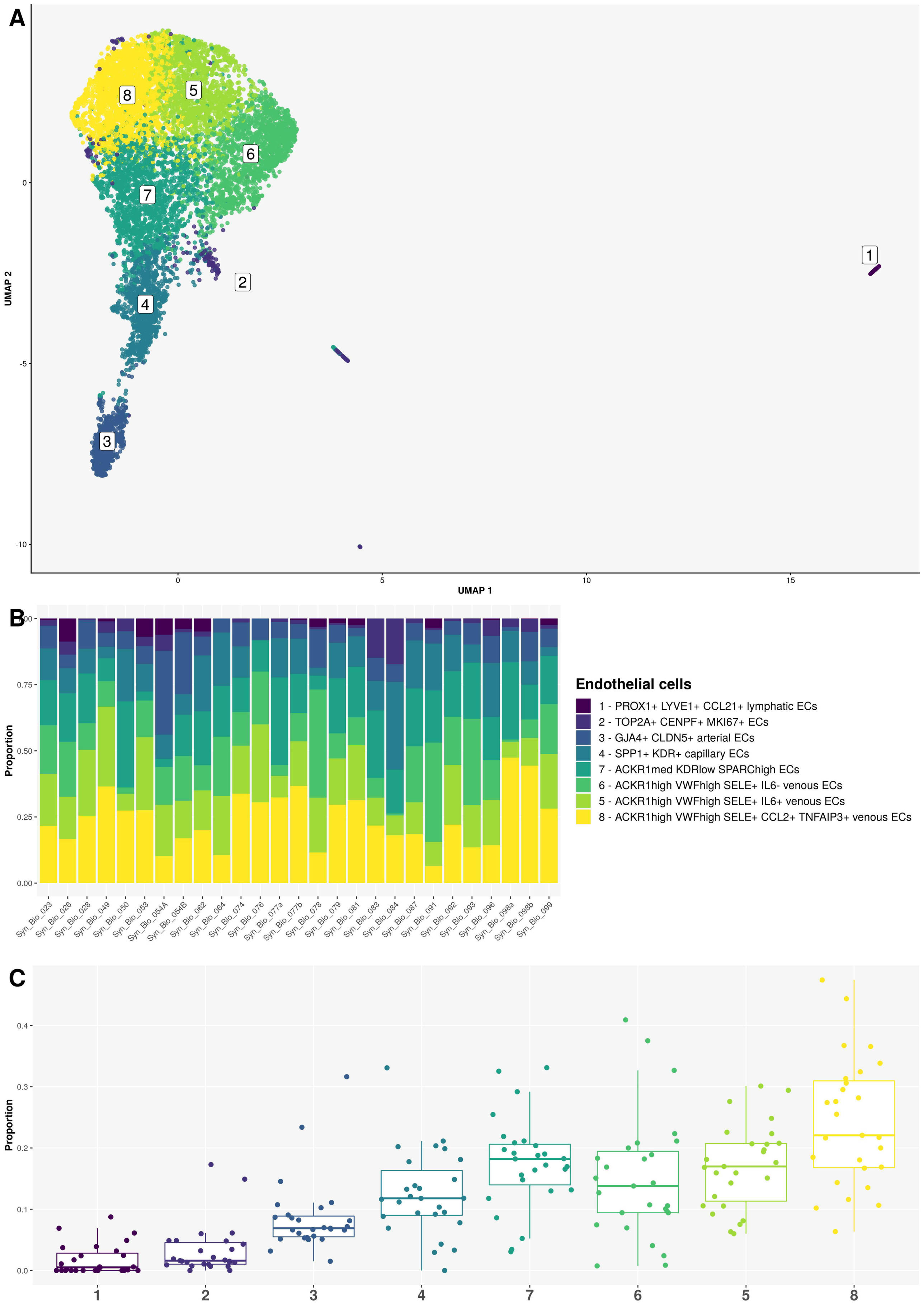
A
UMAP 2
UMAP 1
0
-5
-10
0
5
10
15
8
5
6
7
2
4
3
1
B
Proportion
0.00
0.25
0.50
0.75
1.00
Syn_Bio_023
Syn_Bio_026
Syn_Bio_028
Syn_Bio_049
Syn_Bio_050
Syn_Bio_053
Syn_Bio_054A
Syn_Bio_054B
Syn_Bio_062
Syn_Bio_064
Syn_Bio_074
Syn_Bio_076
Syn_Bio_077a
Syn_Bio_077b
Syn_Bio_078
Syn_Bio_079
Syn_Bio_081
Syn_Bio_083
Syn_Bio_084
Syn_Bio_087
Syn_Bio_091
Syn_Bio_092
Syn_Bio_093
Syn_Bio_096
Syn_Bio_098a
Syn_Bio_098b
Syn_Bio_099
Endothelial cells
1 - PROX1+ LYVE1+ CCL21+ lymphatic ECs
2 - TOP2A+ CENPF+ MKI67+ ECs
3 - GJA4+ CLDN5+ arterial ECs
4 - SPP1+ KDR+ capillary ECs
7 - ACKR1med KDRlow SPARChigh ECs
6 - ACKR1high VWFhigh SELE+ IL6- venous ECs
5 - ACKR1high VWFhigh SELE+ IL6+ venous ECs
8 - ACKR1high VWFhigh SELE+ CCL2+ TNFAIP3+ venous ECs
C
Proportion
0.0
0.1
0.2
0.3
0.4
1
2
3
4
7
6
5
8

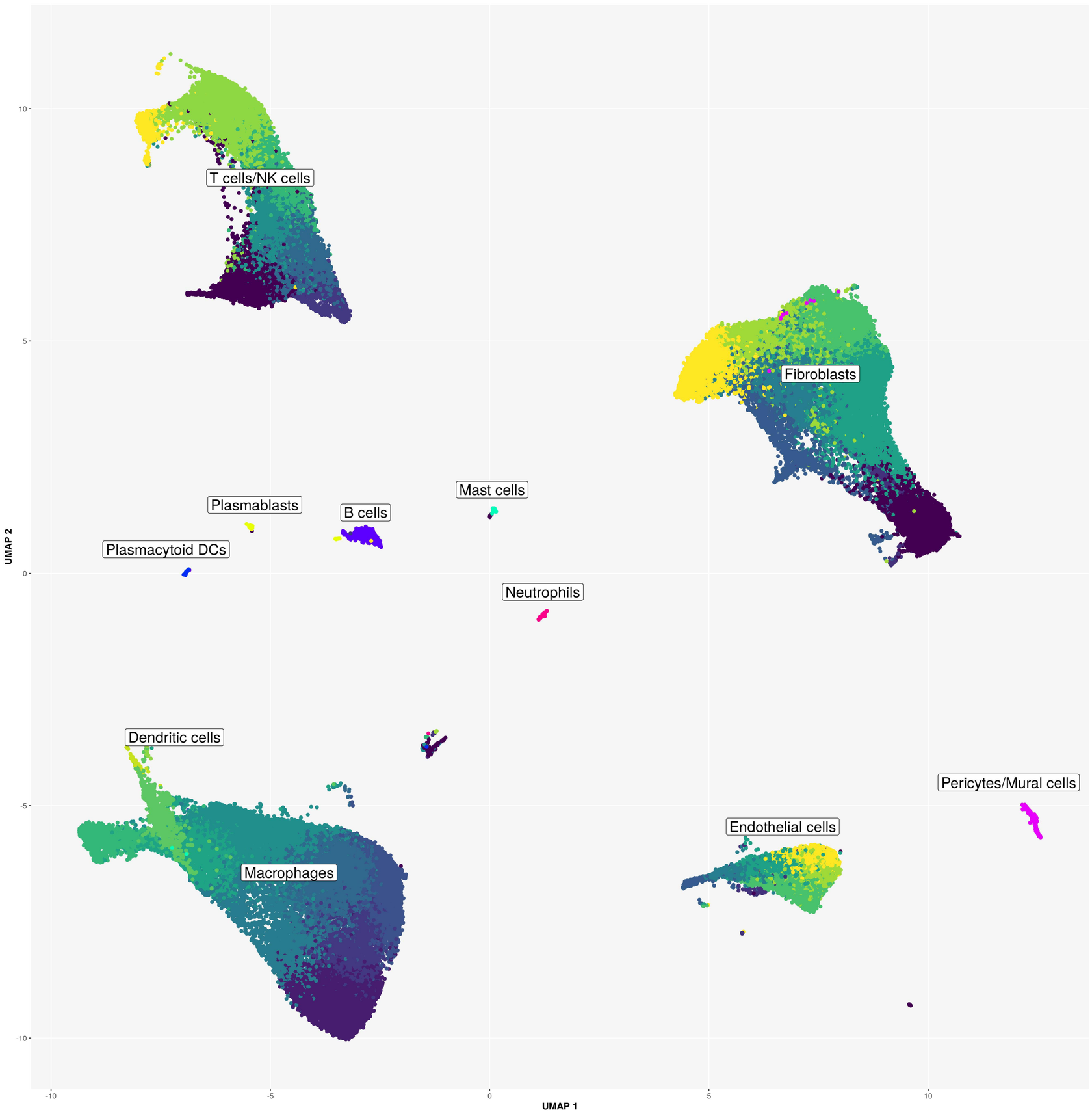

B cells

- B cells

Endothelial cells

- SPP1+ KDR+ capillary ECs
- PROX1+ LYVE1+ CCL21+ lymphatic ECs
- ACKR1med KDRlow SPARChigh ECs
- ACKR1high VWFhigh SELE+ IL6- venous ECs
- ACKR1high VWFhigh SELE+ CCL2+ TNFAIP3+ venous ECs
- GJA4+ CLDN5+ arterial ECs
- ACKR1high VWFhigh SELE+ IL6+ venous ECs
- TOP2A+ CENPF+ MKI67+ ECs

Macrophages

- TIMD4+ TREM2+ LYVE1low IGF1-
- TIMD4+ TREM2+ LYVE1low EGR1-
- TIMD4- TREM2- LYVE1high CD209high
- CX3CR1+ CD48low CLEC10A+
- CX3CR1- SPP1+ TREM2+
- TIMD4+ TREM2+ LYVE1med
- COLEC12- transitional
- CX3CR1+ CD48high CD52high S100A12+
- FOL2R+ MERTK- CD206-

Fibroblasts

- HLA-DRAhigh
- GGT5high CXCL12high FGF7+
- CLIC5+ HBEGF+
- SCD4+ SAA1+ SAA2+
- NOTCH3+ GGT5low
- TNXBhigh GFBP6+ FGFBP2+
- SERPINE1 + COL5A3+
- CADM1high ACAN+

T cells/NK cells

- NKG7+ GNLY+/- GZMKhigh/low
- CCR7low/- LEFFlow SELL-
- CCR7med LEFFmed SELLmed
- CCR7high LEFFhigh SELLhigh
- NKG7low GZMK+
- FOXP3+ CXCL13+ PDCD1+
- CD3- NKG7high GNLYhigh NK cells

Plasmablasts

- Plasmablasts

Dendritic cells

- CD1C+ CLEC10A+
- LAMP3+ IDO1+
- CLEC9A+ CADM1+ CLNK+

Pericytes/Mural cells

- Pericytes/Mural cells

Mast cells

- Mast cells

Plasmacytoid DCs

- LILRA4+ GZMB+ ITM2C+ plasmacytoid

Neutrophils

- Neutrophils